RSC Advances

PAPER

View Article Online
View Journal | View Issue

Cite this: *RSC Adv.*, 2026, **16**, 28113

A chitosan/rGO/Fe_3O_4-modified electrode for sensitive cholesterol determination in blood serum

Irwana Nainggolan, *[abc] Tulus Ikhsan Nasution, [cd] Sake Juli Martina,[e] Agung Pratama, [f] Bing Li,[g] Maya Safrina Dalimunthe,[a] Ardiansyah Sembiring, [abch] Reka Mustika Sari, [i] Khatarina Meldawati Pasaribu, [j] Hanip Fahri,[k] Rica Asrosa,[e] Rozyanty Rahman,[l] Marlin Ramadhan Baidillah [m] and Susilo Sudarman [n]

Cholesterol (Ch) plays a crucial role in the cell membrane structure and metabolic processes, including hormone and bile acid biosynthesis. However, an abnormally high Ch level in the blood is a major risk factor for cardiovascular disease, the leading cause of global mortality, highlighting the need for accurate and sensitive Ch detection. In this study, we designed a straightforward, cost-effective, and robust quantitative approach for Ch detection using a chitosan/reduced graphene oxide/magnetite (CS/rGO/Fe_3O_4)-modified copper-printed circuit board (Cu-PCB) electrode. The proposed electrode was fabricated by depositing a CS/rGO/Fe_3O_4 composite onto Cu-PCB's surface *via* the electrodeposition technique. The obtained electrode was characterized using Fourier transform infrared (FTIR) spectroscopy, X-ray diffraction (XRD), Raman spectroscopy, field-emission scanning electron microscopy (FESEM), atomic force microscopy (AFM), and cyclic voltammetry (CV) techniques. The proposed electrode was used for the detection of cholesterol *via* CV, which exhibited a linear range of 100–300 mg dL^{-1}, sensitivity of 0.160 μA μM^{-1} cm^{-2}, limit of detection of 0.149 μM, and limit of quantification of 0.496 μM. The fabricated electrode also displayed satisfactory results when detecting cholesterol in blood serum samples compared with conventional laboratory analysis. Finally, the developed electrode showed excellent agreement with laboratory reference methods (R^2 = 0.99947), confirming the accuracy and practical applicability of the proposed platform for serum cholesterol analysis.

Received 26th November 2025
Accepted 13th April 2026

DOI: 10.1039/d5ra09147k

rsc.li/rsc-advances

[a]*Department of Chemistry, Faculty of Mathematics and Natural Science, Universitas Sumatera Utara, Medan, 20155, Indonesia. E-mail: irwana@usu.ac.id*
[b]*Center of Excellent Chitosan and Advance Materials, Universitas Sumatera Utara, Medan, 20155, Indonesia*
[c]*Center of Excellent for Greenhouse Gas Emission Control, Universitas Sumatera Utara, Medan, 20155, Indonesia*
[d]*Department of Physics, Faculty of Mathematics and Natural Science, Universitas Sumatera Utara, Medan, Sumatera Utara, 20155, Indonesia*
[e]*Department of Pharmacology and Therapeutics, Faculty of Medicine, Universitas Sumatera Utara, Medan, Indonesia*
[f]*Department of Chemistry, Faculty of Vocational, Universitas Sumatera Utara, Medan, 20155, Indonesia*
[g]*Institute for Materials Discovery, University College London, London, WC1E 7JE, UK*
[h]*Postgraduate School, Department of Chemistry, Faculty of Mathematics and Natural Sciences, Universitas Sumatera Utara, Medan, 20155, Indonesia*
[i]*Research Center for Food Technology and Processing, National Research and Innovation Agency, Gunungkidul, Yogyakarta, Indonesia*
[j]*Research Center for Biomass and Bioproducts, National Research and Innovation Agency of Indonesia (BRIN), Cibinong, 16911, Indonesia*
[k]*RSUD Drs. H. Amri Tambunan, Deli Serdang, 20518, Indonesia*
[l]*School of Materials Engineering, Faculty of Chemical Engineering Technology, Universiti Malaysia Perlis, Malaysia*
[m]*Research Center for Electronics, National Research and Innovation Agency (BRIN), KST Samaun Samadikun, Bandung, 40135, Indonesia*
[n]*Research Center for Molecular Chemistry, National Research and Innovation Agency (BRIN), B.J. Habibie Science and Technology Area, South Tangerang, 15314, Indonesia*

1. Introduction

Recently, cholesterol detection in blood serum has become increasingly important due to its potential impact on human health. Cholesterol (Ch) is a lipid compound that serves as a precursor for the synthesis of steroid hormones, bile acids, and vitamin D and facilitates the absorption of fat-soluble vitamins.[1] Despite its health benefits, insufficient amounts of Ch can lead to hypolipoproteinemia, sepsis, starvation, hyperthyroidism, and hepatic illness. In contrast, excessive levels of Ch in the blood are associated with serious health problems, including coronary heart disease (cardiovascular, CVD), stroke, and hypertension.[2] These ailments are the predominant causes of mortality globally. In 2020, the World Health Federation (WHF) reported that around 17.9 million people die every year from cardiovascular disease (CVD).[3] Meanwhile, Indonesia contributed the highest prevalence of death from stroke and CVD, around 19.42% and 14.38%, respectively.[4] Therefore, developing methods that are prompt, precise, and highly sensitive and selective for detecting blood cholesterol levels is essential for preventing and managing the risk of CVD.

Many analytical methods have been developed for detecting and measuring Ch levels, such as fluorescence biosensing,[5,6]

chemiluminescence,[7,8] colorimetry,[9] spectrophotometry, enzymatic method, high-performance liquid chromatography,[10] and electrochemical methods.[11–13] The spectrophotometric and enzymatic methods are not inherently slow, complex, or costly; however, the use of an enzyme immobilised on an electrode surface had limitations because the enzyme is easily denatured during the immobilisation stage.[14] In addition, the fluorescence method has garnered significant attention due to its sensitivity, stability, and ease of operation; however, its application in biological materials is constrained by interference from the inherent fluorescence of biological tissues and scattered light.[6,15] Unlike the previous platforms, electrochemical methods, especially cyclic voltammetry (CV), offer novel approaches for cholesterol detection owing to their practicality, rapidity, cost-effectiveness, and enhanced linearity, limit of detection (LOD), limit of quantification (LOQ), sensitivity and selectivity compared with currently available methods.[12,13,16–18] Furthermore, CV commonly employs three types of electrodes (counter, reference, and working). The principle of CV is related to redox mechanisms, reaction kinetics, and analyte interactions at the working electrode (WE) surface. This technique measures the electric current generated by redox reactions on the surface of an electrode when a potential is repeatedly applied over a certain range. As a result, the obtained electric current will be interpreted as the concentration of the analyte under investigation.[19,20]

Copper printed circuit board-based electrodes (Cu-PCB) have been utilised in electrochemical applications as working electrodes (WE), especially in biomolecule detection, due to their low cost, ease of fabrication, and compatibility with miniaturized sensing platforms.[21,22] In an effort to enhance the detection efficacy, surface modification of the WE is required. To date, the use of metal-oxide nanomaterials as electrode modifiers has been popular because of their chemical stability and electrocatalytic properties, which can promote electron transfer during redox reactions and consequently improve the detection sensitivity.[23]

Among various chemical materials, the application of metal oxide-based materials for Ch detection is attracting substantial interest because of the superior electrocatalytic capabilities, remarkable chemical stability, and ability to enhance electron transfer during redox reactions.[24,25] Moreover, these phenomena can improve the detection sensitivity. The metal oxides that have been utilised for Ch detection include ZnO,[26] TiO_2,[27] Fe_3O_4,[28] CuO,[29] Cu_2O,[30] Cu_2S,[31] NiO,[32] and SnO_2 (ref. 33) due to their wide band gap. However, although several CS/rGO/metal oxide composites have been reported, the specific role of Fe_3O_4 within this framework has not been systematically investigated. Owing to its mixed-valence Fe^{2+}/Fe^{3+} structure and relatively high electrical conductivity, Fe_3O_4 may act as an efficient mediator for interfacial electron transfer, thereby improving the electrochemical response of the sensing platform.

Magnetite (Fe_3O_4) has attracted significant attention for cholesterol (Ch) sensing owing to its favourable biocompatibility, low toxicity, superparamagnetic behaviour, and facile synthesis. Fe_3O_4 is a semiconductor material with a moderate band gap ($E_g \approx 2.08$ eV at 300 K), enabling its use in electrochemical sensing applications. The presence of Fe^{2+}/Fe^{3+} redox couples within its crystal structure facilitates efficient electron exchange, thereby enhancing the electrochemical oxidation response to target analytes.[34] However, despite its advantages, Fe_3O_4-based cholesterol detection often suffers from poor reproducibility and interference effects arising from the non-specific adsorption of proteins, glucose, and metal ions in complex biological matrices such as blood serum, which can reduce the detection accuracy and sensitivity.

To address these challenges, Fe_3O_4-based Ch detection can be achieved by adding carbon-based nanomaterials, surface functionalisation with organic ligands, or immobilized within polymeric matrices. Therefore, adding carbon-based nanomaterials such as rGO is required to enhance the efficacy of Fe_3O_4.

In recent years, reduced graphene oxide (rGO) has attracted attention because of its exceptional electrical conductivity, large active surface area, and excellent charge-transfer capability.[35–37] rGO is an aromatic carbon single-layer nanomaterial, which is composed of sp^2-hybridised carbon atoms arranged in a honeycomb lattice configuration.[38] In addition, rGO has favourable biocompatibility, high chemical stability, and ease of functionalisation.[39] In 2019, Phetsang *et al.* reported that the functionalization and combination of rGO with metal oxides can significantly improve the electrochemical performance of composites compared to single components.[40] Thereby, integrating rGO and Fe_3O_4 can improve the conductivity and interfacial electron-transfer kinetics of composite materials in detecting Ch. However, the direct applying of Fe_3O_4/rGO nanocomposite into Cu-PCB substrates presents significant challenges regarding poor adhesion and mechanical stability, which can compromise sensor reproducibility during electrochemical measurements.

To overcome these limitations, chitosan (CS) is introduced as a functional polymeric matrix. CS is a naturally abundant biopolymer composed of D-glucosamine and *N*-acetyl-D-glucosamine units and is well known for its excellent film-forming ability, biocompatibility, non-toxicity, and mechanical robustness. Importantly, CS facilitates the strong adhesion of nanomaterials to the surface of electrodes and provides functional groups capable of chelating metal oxides, thereby enhancing the stability of composites.

In this work, CS is employed to immobilize Fe_3O_4/rGO composites onto a Cu-PCB electrode, forming a stable and conductive sensing interface. Within this composite, Fe_3O_4 primarily functions as an electron-transfer mediator that promotes surface-assisted cholesterol oxidation, rGO provides efficient charge-transport pathways, and CS ensures structural stability and reproducibility, particularly in serum-based measurements. Therefore, the rational integration of CS, rGO, and Fe_3O_4 is motivated by the need to overcome the stability, interference, and reproducibility limitations of existing non-enzymatic Ch sensors, enabling the sensitive and reliable Ch detection.

Next, ionic gelation and stirring methods were utilised to combine CS, rGO, and Fe_3O_4 due to its simplicity, ease of

control, and ability to produce a homogeneous composite and enhance electron affinity during the reaction.[41,42] Meanwhile, the resulting CS/rGO/Fe_3O_4 composite was further deposited onto the sensitive area of the Cu-PCB-based WE using the electrodeposition technique.

The electrodeposition technique has been widely applied for depositing various materials, such as metals, metal oxides, and composites onto the surface of electrodes through electrochemical reactions in an electrolyte containing the target ions.[43,44] Interestingly, this technique has several benefits, including straightforward and time-efficient procedure and low cost. Likewise, this method can control the layer thickness and morphology using the current, potential, deposition time, and the solution concentration is also managed.[43]

Previous studies have reported diverse methodologies for detecting cholesterol in blood serum *via* electrochemical techniques, achieving high sensitivity, rapid response time, and low sample consumption. Nainggolan *et al.* reported the detection of Ch based on a chitosan/reduced graphene oxide/manganese dioxide-modified electrode.[13] Furthermore, Willyam *et al.* reported the use of β-cyclodextrin/Fe_3O_4 nanocomposites for the fabrication of an electrochemical non-enzymatic cholesterol sensor, where the BCD/Fe_3O_4 nanocomposite exhibited a linear range of 0–150 μM and an LOD of 2.88 μM.[45] In addition, the electrochemical detection of Ch was performed using Fe_3O_4/APTES/PAMAM.[46] In another study, Ch measurements were conducted using CIT-BCD@Fe_3O_4 based on electrochemical and computational studies with an LOD value of 3.93 μM.[47]

Despite these advances, challenges related to electrode stability, interfacial charge-transfer efficiency, and reproducibility in complex biological matrices remain. In this report, we

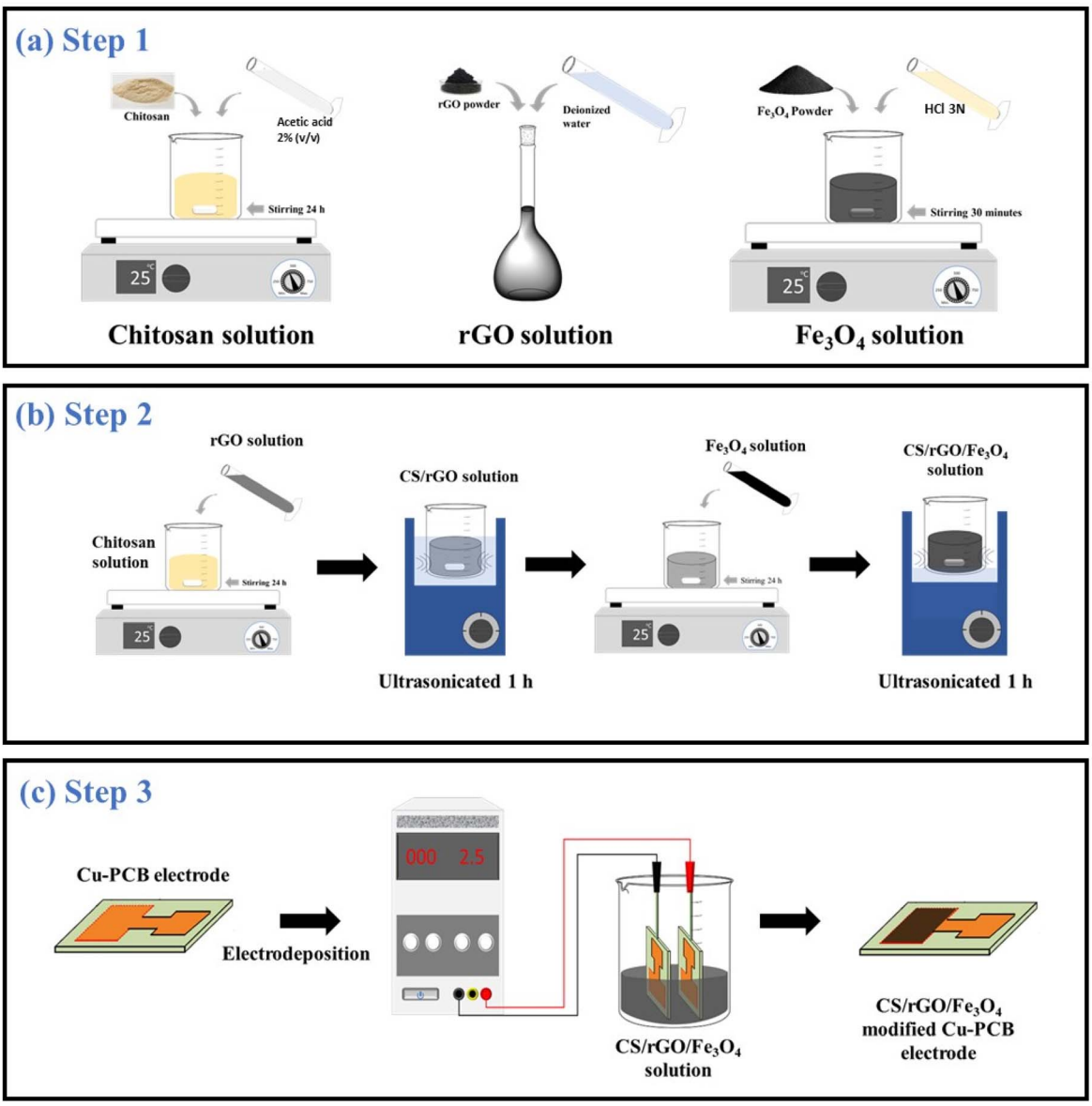

Fig. 1 Schematic of the synthesis of the CS/rGO/Fe_3O_4-modified Cu-PCB electrode: (a) preparation of the CS, rGO and Fe_3O_4 solutions, (b) preparation of the CS/rGO/Fe_3O_4 composite, and (c) fabrication of the CS/rGO/Fe_3O_4-modified Cu-PCB.

designed an approach to detect the Ch concentration in blood serum using a chitosan/rGO/Fe_3O_4 composite-modified Cu-PCB electrode. The fabricated electrode was systematically characterised to determine its structural and morphological properties, and its electrochemical performance was evaluated to assess its suitability for sensitive and reliable cholesterol detection.

2. Experimental

2.1 Material

The copper PCB substrate was obtained from Commanditaire Vennootschap (CV) Al-Tronic, Medan, Indonesia. Additionally, commercial cholesterol reagent, hydrochloric acid (HCl), glacial acetic acid (CH_3COOH), phosphate buffer saline (PBS) solution pH 7, and deionized water (DI) were purchased from Merck. Chitosan, magnetite (Fe_3O_4), and reduced graphene oxide (rGO) were procured from Sigma-Aldrich. Blood serum samples containing cholesterol were donated by Drs. H. Amri Tambunan Hospital, Deli Serdang, Indonesia.

2.2 Preparation of CS/rGO/Fe_3O_4 composite

In this step, ionic gelation and stirring methods were utilised to prepare the CS, rGO, and Fe_3O_4 solutions (Fig. 1a). Briefly, 1.5 g of CS powder was dissolved in 100 mL of 2% (v/v) CH_3COOH and stirred on a magnetic stirrer at room temperature for 24 h. The obtained CS solution was sonicated at 20 kHz for 1 h and then kept in a cooling room at approximately 4 °C–8 °C. Secondly, an rGO suspension (1%, (1 mg mL^{-1})) was diluted using deionized water to obtain 250 mg L^{-1} rGO, where 25 mL of 1% rGO suspension was added to 100 mL of deionized water. After that, the resulting 250 mg L^{-1} rGO solution was homogenised and sonicated at 20 Hz for 2 h. The determination of an rGO concentration of 250 mg L^{-1} was supported by earlier research conducted by Sembiring *et al.* (2023)[48] and Nainggolan *et al.* (2024),[13] which indicated that this concentration represents the optimal condition for utilising rGO as a sensing material in electrochemical applications. Furthermore, a solution of 75 mg L^{-1} Fe_3O_4 was prepared by dissolving 3.75 mg of Fe_3O_4 powder in 50 mL of 37% (v/v) HCl and then stirring at room temperature for 30 min. A similar method was employed to prepare Fe_3O_4 solutions with concentrations of 90, 105, and 120 mg L^{-1}.[13]

The CS/rGO/Fe_3O_4 composites were prepared by mixing 10 mL of CS solution and 10 mL of rGO solution under continuous stirring at 200–300 rpm for 24 h, followed by ultrasonication for 1 h. Next, the prepared CS/rGO composite was added to the Fe_3O_4 solution at the concentrations specified in Table 1 under continuous stirring at 200–300 rpm for 24 h, followed by ultrasonication.[13] A schematic of the preparation of the CS/rGO/Fe_3O_4 composite is displayed in Fig. 1b.

Table 1 Composition of the CS/rGO/Fe_3O_4 composite

CS (%)	rGO (mg L^{-1})	Fe_3O_4 (mg L^{-1})
10 mL	(10 mL)	(10 mL)
1.5	250	75
1.5	250	90
1.5	250	105
1.5	250	120

2.3 Fabrication of chitosan/rGO/Fe_3O_4-modified copper printed circuit board electrode

Firstly, the Cu-PCB substrate used for electrode fabrication was prepared with dimensions of 15 mm × 15 mm × 2 mm. The exposed working electrode area was defined as 35 mm^2 (0.35 cm^2) and served as the geometric surface area in contact with the electrolyte. This area was kept constant for all experiments to ensure consistent impedance behavior and reliable comparison of electrochemical responses. The CS/rGO/Fe_3O_4-modified Cu-PCB electrode was fabricated *via* the electrodeposition method. Briefly, 20 mL of CS/rGO/Fe_3O_4 composite was prepared in a 50 mL glass beaker. Next, the electrodeposition equipment was assembled, with a two-electrode configuration, consisting of an anode and a cathode, as shown in Fig. 1c. After that, the unmodified Cu-PCB electrode was positioned between the cathode and anode sides at room temperature. During the electrodeposition process, electrical current was flowed at a voltage of 2.5 V for 5 min. Initially, the current increased due to charge transfer and nucleation at the electrode–electrolyte interface, followed by a gradual decrease and stabilization in the ampere range (approximately 10^{-4}). The quasi-steady current behavior suggests the formation of a uniform and stable composite layer on the Cu-PCB working electrode. Next, the resulting CS/rGO/Fe_3O_4-modified Cu-PCB electrode was dried in an oven at 60 °C for 60 min.

2.4 Commercial cholesterol reagent and blood serum preparation

Firstly, 5 mL of commercial cholesterol reagent was diluted using 50 mL of phosphate buffer solution (PBS, pH = 7.0). Following that, various concentrations of Ch (100, 150, 200, 250, and 300 mg dL^{-1}) were prepared. These concentrations were selected to ensure relevance to physiological conditions while maintaining a linear electrochemical response. Meanwhile, blood serum samples were used as real samples and were directly analyzed without the addition of cholesterol reagent. Prior to measurement, the serum samples were gently homogenized and subjected to cyclic voltammetry and electrochemical impedance spectroscopy under the same experimental conditions as the standard solutions. The cholesterol concentrations obtained from the electrochemical measurements of blood serum were compared with the corresponding laboratory reference values to evaluate the accuracy of the proposed sensor.

2.5 Characterisation

To determine the functional groups present in the samples, they were characterized using a Fourier-transform infrared (FTIR) spectrophotometer (IR Prestige-21 Shimadzu, Japan) at the Integrated Laboratory of Lampung University, Indonesia. The scans were conducted at wavenumbers ranging from 450–

4000 cm^{-1}. The structural properties of the synthesized materials were examined using X-ray diffraction (XRD) on a Bruker AXS D8 Advance diffractometer employing Cu Ka radiation (λ = 1.5406 Å) at the Integrated Laboratory of Kalimantan Institute of Technology, Indonesia. Raman spectra were recorded using a LabRAM HR Evolution Raman Spectrometer from HORIBA Scientific with a 532 nm excitation laser at the Cryo EM Laboratories-RAMAN, National Research and Innovation Agency, Indonesia. In addition, field-emission scanning electron microscopy-energy dispersive X-ray (FESEM-EDX) spectroscopy analysis was performed to observe the microscopic deformation of each sample. In this study, the FESEM images were recorded using a Bruker microscope at an accelerating voltage of 10.0 kV. The assessment of the topographical of the modified Cu-PCB electrode was carried out utilising atomic force microscopy (AFM, Park NX10 type) operated in non-contact mode. Topographic images were acquired over a 5 μm × 5 μm area with high resolution, enabling visualisation of surface features in detail down to the nanometer scale.

2.6 Electrochemical performance determination

Electrochemical testing of the modified Cu-PCB electrode was carried out utilising cyclic voltammetry (CV) with a CorrTest Electrochemical Workstation at the Analytical Laboratory, Faculty of Mathematics and Natural Sciences, Universitas Sumatera Utara, Indonesia. The CV setup consisted of a three-electrode system comprising a reference electrode (Ag/AgCl), an auxiliary electrode (Pt) and a working electrode (chitosan/rGO/Fe_3O_4-modified Cu-PCB). The experimental configuration involved a potential window of −1 V to +1 V. Subsequently, PBS (pH = 7) was used as the supporting electrolyte for initial tests at scan rates of 50, 75, and 100 mV s^{-1}. After that, the optimum scan rate and modified electrodes were used to evaluate the electrochemical properties in various concentrations of commercial Ch reagent and blood serum containing Ch.

3. Results and discussion

3.1 FTIR analysis

The chemical functional groups in the CS, CS/rGO, and CS/rGO/Fe_3O_4-modified Cu-PCB electrodes were analysed using FTIR spectroscopy. Fig. 2a–c present the spectra of pure CS, the CS/rGO-modified Cu-PCB electrode, and the CS/rGO/Fe_3O_4-modified Cu-PCB electrode, respectively. Fig. 2a displays absorption bands at 3442.9 cm^{-1}, 2079 cm^{-1}, 1637.5 cm^{-1}, and 1278.8 cm^{-1} corresponding to hydroxyl groups, C–H bonds in –CH_2, amide I, and C–H functional group, respectively, demonstrating the properties of pure CS. After incorporating rGO into the CS matrix, the CS/rGO-modified Cu-PCB electrode (Fig. 2b) showed a noticeable change in the O–H stretching region at 3450.6 cm^{-1}. This modification is commonly associated with hydrogen-bond interactions between the hydroxyl groups of CS and the oxygen-containing functional groups of rGO, suggesting a physical interaction between the two components rather than the formation of new covalent bonds.[12,49] Therefore, these results confirm that rGO is well distributed within the CS matrix. On the other hand, the FT-IR spectrum of the CS/rGO/Fe_3O_4-modified Cu-PCB electrode (Fig. 2c) shows an absorption band at approximately 549.7 cm^{-1}, which is attributed to Fe–O stretching vibrations. This characteristic band qualitatively confirms the incorporation of Fe_3O_4 into the CS/rGO composite. In addition, the overall FTIR spectral features remain consistent with those of CS-based composites, indicating that Fe_3O_4 and rGO are successfully embedded within the chitosan matrix without altering its fundamental chemical structure.[50] Collectively, the FTIR results provide qualitative evidence supporting the successful formation and deposition of the CS/rGO/Fe_3O_4 composite on the Cu-PCB electrode. Further structural, morphological, and electrochemical characterizations were performed to evaluate the properties of the fabricated electrodes.

3.2 XRD analysis

XRD was performed to study the crystallographic structure of the samples. The XRD patterns of CS, the CS/rGO-modified Cu-PCB electrode, and the CS/rGO/Fe_3O_4-modified Cu-PCB electrode are presented in Fig. 3. Fig. 3a shows the XRD pattern of CS, where the broad peak indicates that CS has a semi-crystalline structure due to intramolecular and intermolecular hydrogen interactions in the polysaccharide chain. The main peak at around 20° corresponds to the (110) crystalline plane.[51] Furthermore, the XRD pattern of the CS/rGO-modified Cu-PCB electrode is similar to that of pure CS, showing only one broad diffraction peak at 2θ = 21.1°, which corresponds to the

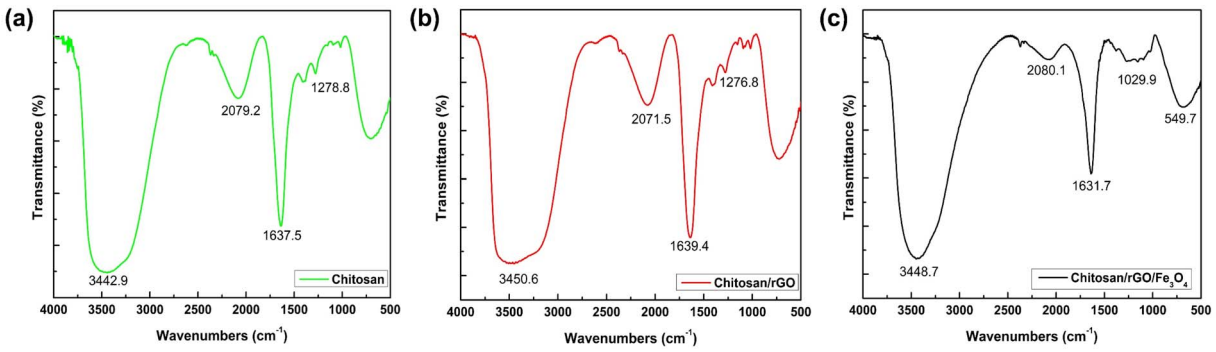

Fig. 2 FT-IR spectra of (a) pure CS, (b) the CS/rGO-modified Cu-PCB electrode, and (c) the CS/rGO/Fe_3O_4-modified Cu-PCB electrode.

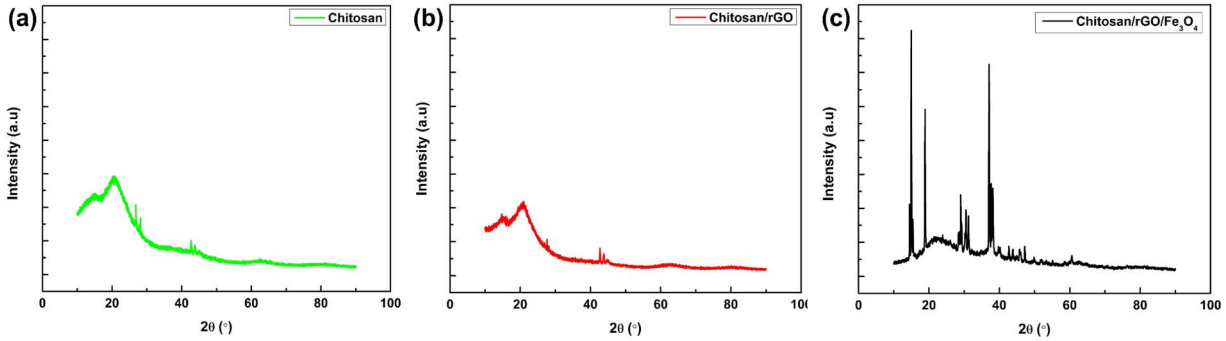

Fig. 3 XRD patterns of (a) pure CS, (b) the CS/rGO-modified Cu-PCB electrode, and (c) the CS/rGO/Fe_3O_4-modified Cu-PCB electrode.

amorphous state of CS (Fig. 3b). The absence of the typical rGO peak indicates that the regular and periodic structure of rGO becomes more disordered due to the formation of a randomly oriented 3D network. In addition, the incorporation of rGO into the CS matrix has little effect on the crystalline properties of CS, indicating that most physical interactions occur between rGO and CS.[52] Next, the XRD pattern shows peaks at $2\theta = 14°$ and 20°, which indicate that the nanocomposite still maintains its crystallinity.[12] Following the introduction of Fe_3O_4 into the CS/rGO composite (Fig. 3c), sharp diffraction peaks are observed at $2\theta \approx 30.41°$, 36.5°, 42.7°, 53.5°, 58.39°, and 60.4°, which correspond to the (220), (311), (400), (422), (511), and (440) crystal planes[34,53,54] of the face-centered cubic (FCC) structure of Fe_3O_4, respectively.[55,56] These peaks are consistent with the standard pattern for crystalline magnetite with a spinel structure. This indicates that CS modification does not cause a change in the Fe_3O_4 phase.[57] Moreover, the changes in the XRD pattern of CS indicate the successful CS/rGO/Fe_3O_4 copolymerization. The results indicate that the composite exists in crystalline form.

3.3 Raman analysis

Raman analysis was performed to identify the chemical structure and interactions between the components in the CS, CS/rGO, and chitosan/rGO/Fe_3O_4 materials,[58] as presented in Fig. 4a–c, respectively. Based on the obtained spectra, pure CS shows a peak at 1348 cm^{-1}, corresponding to the deformation vibration (CH_2).[59,60] Meanwhile, the Raman signal for the amine group (NH_2) in CS is located at 1593 cm^{-1}.[61] The signals in the range of 2800–3000 cm^{-1} usually originate from the stretching vibration of the CH or CH_2 groups.[62] These peaks indicate the presence of an intact natural polymer structure, including –OH and –NH_2 groups, which are the main characteristics of CS. This is in line with reports that chitosan has characteristic vibrational bands associated with C–H, C–O, and NH_2 groups in its vibrational spectrum. The high intensity of the peaks in the spectrum of chitosan indicates that this material has many active vibrational modes, thus producing strong Raman signals.

In the chitosan/rGO sample (Fig. 4b), two important peaks appear at around 1350 cm^{-1} (D band) and 1582 cm^{-1} (G band), although with relatively low intensity. The D band is related to structural defects (disorder) in carbon, while the G band is related to the hexagonal lattice vibrational mode of graphite.[63] The presence of these two bands is evidence that rGO has been successfully integrated into the CS matrix.

Furthermore, the Raman spectrum of the chitosan/rGO/Fe_3O_4 composite shows a combination of the characteristics of all its components (Fig. 4c). The D and G bands of rGO are still present, indicating that the graphitic structure is maintained. In addition, a peak appears in the region of 580–700 cm^{-1}, arising from Fe–O vibrations, which is a characteristic of Fe_3O_4 (magnetite). The presence of these peaks confirms that the Fe_3O_4 nanoparticles have been successfully integrated into the composite system. Fe–O vibrations in this range have been reported as a key indicator of the presence of an Fe_3O_4 phase in various graphene-based composites.[64] In addition, the shifts in the peak position and intensity changes indicate the presence of

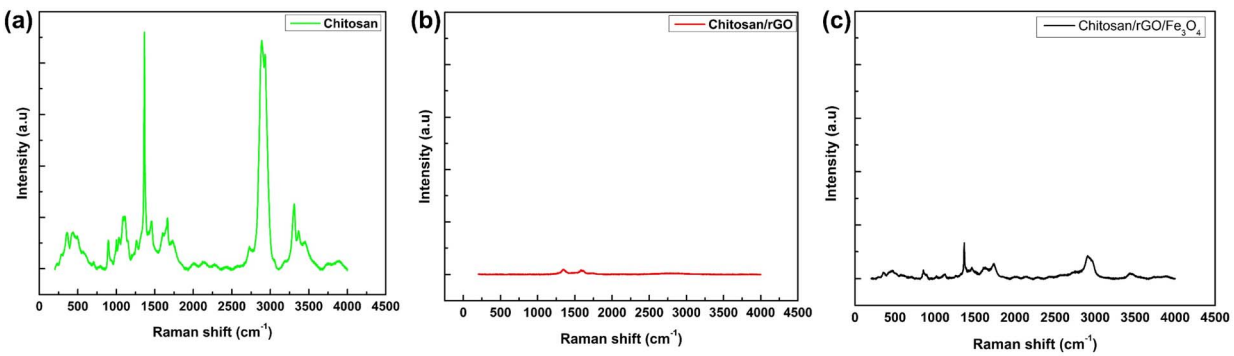

Fig. 4 Raman spectra of (a) pure CS, (b) the CS/rGO-modified Cu-PCB electrode, and (c) the CS/rGO/Fe_3O_4-modified Cu-PCB electrode.

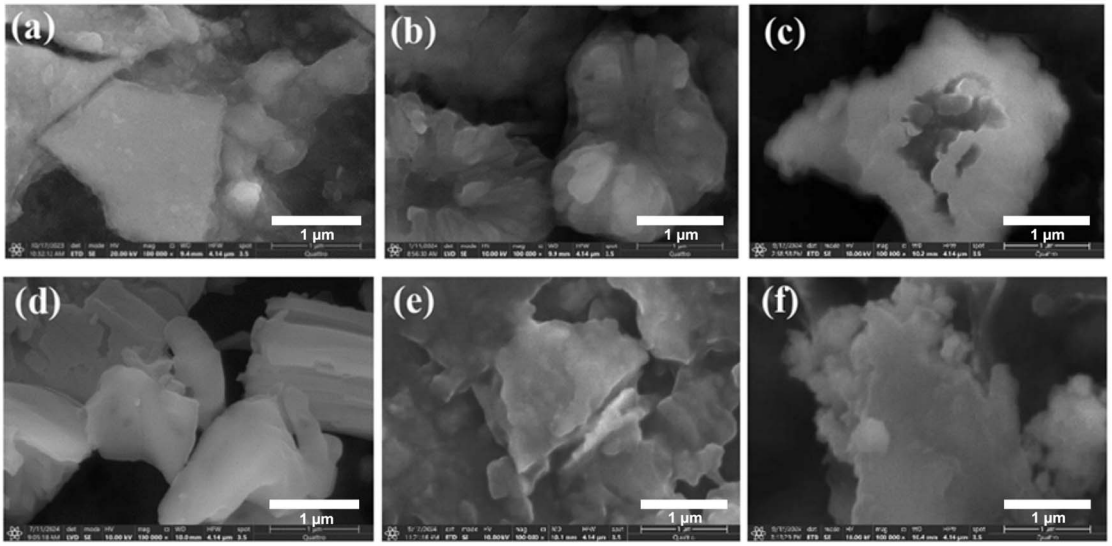

Fig. 5 FE-SEM images of (a) CS, (b) the CS/rGO-modified C-PCB electrode, (c) the CS/rGO/Fe_3O_4-modified Cu-PCB electrode with 75 mg L^{-1} Fe_3O_4, (d) the CS/rGO/Fe_3O_4-modified Cu-PCB electrode with 90 mg L^{-1} Fe_3O_4, (e) the CS/rGO/Fe_3O_4-modified Cu-PCB electrode with 105 mg L^{-1} Fe_3O_4, and (f) the CS/rGO/Fe_3O_4-modified Cu-PCB electrode with 120 mg L^{-1} Fe_3O_4.

chemical interactions between the components, such as cross-linking between CS and rGO, which can be explained by the slight shift in the N–H bending peak from 1665 to 1582 cm^{-1}, and further support the fact that CS, containing O–H and N–H groups, can interact with rGO through electrostatic interactions.[65]

3.4 FESEM-EDX studies

Fig. 5 presents the microscopic morphology of CS, the CS/rGO-modified Cu-PCB electrode, and the CS/rGO/Fe_3O_4-modified Cu-PCB electrode at 1 000 00× magnification, indicating the presence of major gaps. Fig. 5a illustrates that pure CS exhibits a smooth surface with a uniform structure. In addition, it has small pores, making it an ideal base for combining with other materials, such as rGO or Fe_3O_4, to improve its functional properties. On the other hand, the introduction of rGO caused the surface structure of CS to become rougher, as shown in Fig. 5b. This is because the rGO layers distributed on top of the CS matrix, signifying that the hydroxyl and amino groups in CS establish physical interactions (hydrogen bonds) with the oxygen-containing functional groups in rGO. However, this phenomenon does not change the performance of the CS/rGO composites; fortunately, rGO can increase the surface area of these materials, increasing their potential for sensor applications, especially in detecting Ch.[12] Conversely, Fig. 5c–f reveal more complex images, exhibiting the successful fabrication of the CS/rGO/Fe_3O_4-modified Cu-PCB electrodes. It is possible that there are intense physical interactions among CS, rGO and Fe_3O_4. Additionally, these characteristics are also influenced by the superparamagnetic property of Fe_3O_4. Nevertheless, the surface roughness does not have a substantial impact on the efficacy of the CS/rGO/Fe_3O_4-modified Cu-PCB electrode in Ch detection. Instead, it will enhance its potential for detecting Ch.

The elemental composition of the prepared materials was analyzed *via* EDX, as shown in Fig. 6, and the quantitative results are summarized in Table S1 (see the SI), indicating that the pure chitosan film exhibits carbon and oxygen contents of 52.8% and 47.2%, respectively. Meanwhile, the contents of hydrogen and nitrogen were not detected due to the limitations of EDX in detecting light elements. Nevertheless, this limitation does not compromise the validity of the compositional analysis, as the detected carbon and oxygen contents remain consistent with the expected theoretical composition of chitosan and its composites when hydrogen and nitrogen are excluded. The relative proportions of carbon and oxygen are in good agreement with literature-reported values, confirming that the fundamental chemical structure of CS is preserved.[66]

Upon the incorporation of rGO into the chitosan matrix, the carbon content significantly increases to 76.4%, accompanied by a decrease in oxygen content to 23.6%. This trend clearly indicates the successful integration of rGO, which is rich in sp^2-hybridized carbon, into the polymer matrix. The reduction in oxygen content also suggests partial removal of oxygen-containing functional groups during the reduction of graphene oxide, enhancing the electrical conductivity of the composite.[67]

For the CS/rGO/Fe_3O_4-modified electrodes, the presence of Fe confirms the successful incorporation of Fe_3O_4 nanoparticles into the composite system. As the Fe_3O_4 concentration increases from 75 to 120 mg L^{-1}, the Fe content gradually rises from 9.4% to 18.3%, accompanied by a systematic decrease in carbon content from 48.3% to 39.1%. This trend reflects the progressive loading of Fe_3O_4 onto the CS/rGO matrix, which partially replaces the carbon-rich components.[34]

Interestingly, the oxygen content remains relatively constant (~42–43%) across all the Fe_3O_4-containing samples, suggesting that the oxygen contributions originate not only from chitosan but also from the Fe_3O_4 structure and residual oxygen

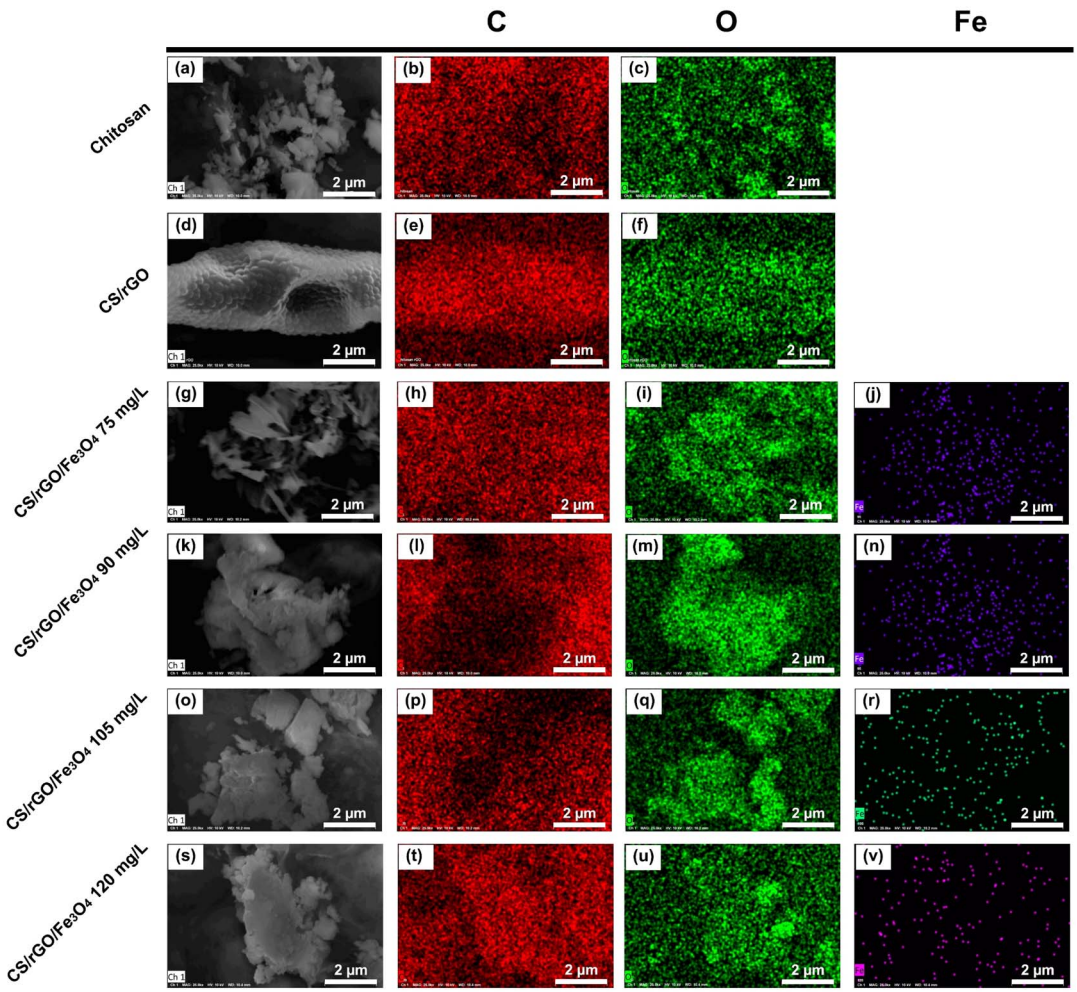

Fig. 6 (a) FE-SEM image of CS and EDS elemental mapping of (b) C and (c) O. (d) FE-SEM image of the CS/rGO-modified Cu-PCB electrode and EDS elemental mapping of (e) C and (f) O. (g) FE-SEM image of the CS/rGO/Fe_3O_4-modified Cu-PCB electrode with 75 mg L^{-1} Fe_3O_4 and EDS elemental mapping of (h) C, (i) O, and (j) Fe. (k) FE-SEM image of the CS/rGO/Fe_3O_4-modified Cu-PCB electrode with 90 mg L^{-1} Fe_3O_4, and EDS elemental mapping of (l) C, (m) O, and (n) Fe. (o) FE-SEM image of the CS/rGO/Fe_3O_4-modified Cu-PCB electrode with 105 mg L^{-1} Fe_3O_4, and EDS elemental mapping of (p) C, (q) O, and (r) Fe. (s) FE-SEM image of the CS/rGO/Fe_3O_4-modified Cu-PCB electrode with 120 mg L^{-1} Fe_3O_4 and EDS elemental mapping of (t) C, (u) O, and (v) Fe.

functional groups in rGO. The stable oxygen percentage indicates that the composite maintains its functional groups, which are essential for interfacial interactions and electrochemical activity.

Overall, the EDX results confirm the successful stepwise formation of CS, CS/rGO, and CS/rGO/Fe_3O_4 composites. The increasing Fe content and corresponding decrease in carbon fraction provide strong evidence of Fe_3O_4 incorporation, while the high carbon content in CS/rGO demonstrates the effective integration of rGO, which is expected to enhance the electron transport properties. These compositional changes are consistent with the improved electrochemical performance observed in subsequent analyses.

3.5 AFM analysis

AFM analysis of the CS/rGO/Fe_3O_4-modified Cu-PCB electrodes was carried out to explore the overall morphological changes in the CS/rGO/Fe_3O_4 composite films due to variations in the Fe_3O_4 concentration. Meanwhile, the AFM topographical images of pure CS and the CS/rGO-modified Cu-PCB electrodes were previously discussed in our earlier publication.[13] The results demonstrated that the topography of pure CS is relatively smooth, while the incorporation of rGO produced a rougher and more irregular morphology due to the electrostatic interaction between the amine groups of CS and the rGO surface, which increased the sheet thickness without altering the rGO monolayer structure. Furthermore, the AFM topographical images of the proposed electrodes are shown in Fig. 7, and the evaluation of the AFM characteristics of the proposed electrodes, involving the areal roughness parameter (S_a), root mean square roughness (RMS/S_q), skewness (S_{sk}), and excess kurtosis (S_{ku}), is summarized in Table S2 (see the SI). Based on Table S2, it can be seen that the S_a and S_q values increase with an increasing Fe_3O_4 concentration from 75 to 120 mg L^{-1}. This indicates that Fe_3O_4 particles play a significant role in forming a rougher and more textured surface due to the increase in the

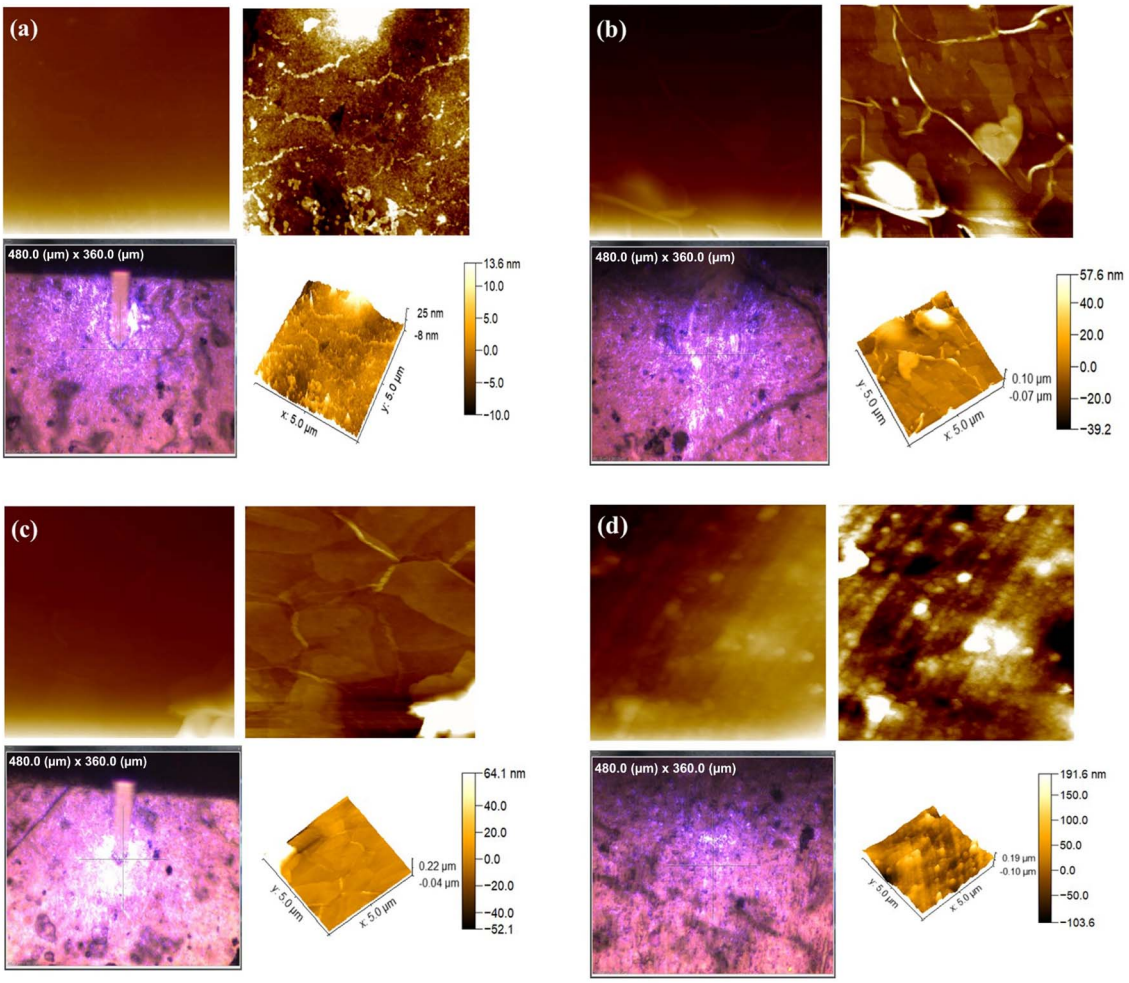

Fig. 7 Topography AFM images of the (a) CS/rGO/Fe_3O_4-modified Cu-PCB electrode with 75 mg L^{-1} Fe_3O_4, (b) CS/rGO/Fe_3O_4-modified Cu-PCB electrode with 90 mg L^{-1} Fe_3O_4, (c) CS/rGO/Fe_3O_4-modified Cu-PCB electrode with 105 mg L^{-1} Fe_3O_4, and (d) CS/rGO/Fe_3O_4-modified Cu-PCB electrode with 120 mg L^{-1} Fe_3O_4.

number of Fe_3O_4 particles distributed in the CS/rGO matrix. At a concentration in the range of 75–90 mg L^{-1}, the S_a value appears relatively moderate, indicating that Fe_3O_4 is still well dispersed in the matrix; however, at elevated concentrations ($\geq$105 mg L^{-1}), there is an increase in the S_a and S_q values, indicating the agglomeration of Fe_3O_4 particles, which results in the appearance of sharp peaks on the surface of the films.

Moreover, the S_{sk} parameter increased from 0.61 to 3.19, confirming the surface roughness trends observed from the S_a and S_q values. A positive S_{sk} indicates that the surface is dominated by protruding peaks rather than valleys. These results are consistent with the findings of Singh *et al.* (2024), who reported that slightly positive S_{sk} values (0–1) enhance the active surface area and adsorption capability, whereas excessively high S_{sk} values (>+1.5) signify Fe_3O_4 agglomeration, which impedes electron transfer. Conversely, negative S_{sk} values describe porous surfaces that may restrict diffusion, while values near zero indicate smooth but less electrochemically active surfaces.[68] Simultaneously, the S_{ku} value increased from 1.83 to 5.6, suggesting that the surface height distribution became more peaked; an $S_{ku} > 3$ denotes the presence of uneven and sharp features associated with nanoparticle aggregation.

Substantially, the incorporation of a moderate concentration of Fe_3O_4 (90–105 mg L^{-1}) into the CS/rGO matrix results in a suitably rough and homogeneous surface, which is optimal for enhancing the active area of the electrode. Conversely, an elevated level of Fe_3O_4 (120 mg L^{-1}) can reduce the homogeneity and efficiency of electron transfer owing to the excessive roughness. Consequently, an Fe_3O_4 concentration of 105 mg L^{-1} was chosen as the optimal level in the CS/rGO matrix for the subsequent electrochemical determination of cholesterol in blood serum samples.

3.6 Electrochemical performance determination

3.6.1 Electrochemical measurement of modified electrode in PBS condition. The optimal modified electrode for measuring cholesterol concentration was identified using the CV technique in PBS (pH 7) at a scan rate of 75 mV s^{-1}. This aims to achieve the optimum composition of the CS/rGO/Fe_3O_4-modified Cu-PCB electrode, along with the determination of the

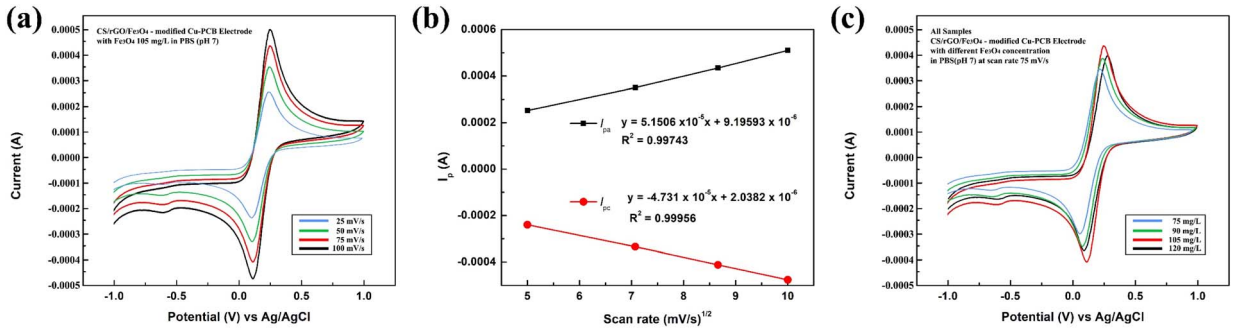

Fig. 8 Effect of scan rate on the detection response of the CS/rGO/Fe_3O_4 electrode (a). Plots of I_{pa} and I_{pc} *vs.* square root of the scan rate (b). Detection responses of all the modified Cu-PCB electrodes (c). All measurements were conducted in PBS (pH 7.0).

most suitable Fe_3O_4 content for further analysis. In this step, all measurements were conducted using three independently prepared electrodes ($N = 3$), and each measurement was performed with three consecutive CV sweeps. The reported data represent the average values obtained under these conditions. The measurement results obtained using CV are displayed in Fig. 8c, while the oxidation and reduction potentials and current values are compiled in Table 2, where I_{pa} is the anodic peak current, I_{pc} is the cathodic peak current, E_{pa} is the anodic peak potential, E_{pc} is the cathodic peak potential, and ΔE_p is the peak-to-peak potential separation.

As shown in Table 2, the anodic (I_{pa}) and cathodic (I_{pc}) peak currents increase significantly with an increasing Fe_3O_4 concentration, indicating enhanced electrochemical activity. This is because of the mixed valence character of Fe_3O_4, which allows rapid electron transfer between the Fe^{2+}/Fe^{3+} redox sites, and thus enhances the charge transfer kinetics.[34] The highest current response is observed at 105 mg L^{-1}, suggesting the optimal Fe_3O_4 loading concentration. However, for the proposed electrode with 120 mg L^{-1} Fe_3O_4, the peak currents slightly decrease, which may be due to particle agglomeration or partial blockage of the active sites, leading to a reduction in the electron-transfer efficiency.

The ratio of anodic to cathodic peak currents ($|I_{pa}/I_{pc}|$) approaches unity (1.053–1.133) with an increasing Fe_3O_4 content, indicating the improved reversibility of the redox process. This is further supported by the decrease in peak separation (ΔE_p) from 0.17 V (75 mg L^{-1}) to 0.13 V (105 mg L^{-1}), suggesting enhanced electron-transfer kinetics. However, the slight increase in ΔE_p at a higher loading (120 mg L^{-1}) indicates a decline in electrochemical performance due to the excessive Fe_3O_4 loading. The small ΔE_p reflects accelerated electron-transfer kinetics, while the high anodic and cathodic peak currents indicate a larger electrochemically active surface area.[69]

Overall, the improved electrochemical performance upon Fe_3O_4 incorporation is mainly attributed to its role in enhancing electron-transfer pathways and increasing the effective surface area of the composite. Rather than acting as a direct catalyst, Fe_3O_4 functions as a conductive mediator within the CS/rGO matrix. However, excessive loading leads to particle aggregation, which hinders charge transport and reduces the electrochemical efficiency.[34]

These findings align with a prior study by Doaga *et al.* (2020), which confirmed that electrodes with an appropriate Fe_3O_4 content exhibit enhanced electrochemical activity and charge transfer efficiency. These electrodes exhibit effective catalysis of cholesterol oxidation and increased sensitivity to cholesterol levels without requiring supplementary measures. These findings highlight that incorporating Fe_3O_4 at an appropriate concentration significantly enhances the electrocatalytic performance of the electrodes.[46]

Finally, the synergistic interaction among chitosan, rGO, and Fe_3O_4 plays a crucial role in enhancing the overall electrochemical performance. CS acts as a flexible polymer matrix that ensures uniform dispersion and strong interfacial adhesion, while rGO provides a highly conductive network that facilitates rapid electron transport. Meanwhile, Fe_3O_4 nanoparticles contribute by increasing the effective surface area and promoting efficient charge-transfer pathways within the composite. This cooperative effect results in improved electron mobility, enhanced interfacial interactions, and an overall superior electrochemical response.

3.6.2 Scan rate study. A scan rate study is important for observing the redox processes, control mechanisms, kinetic parameters, stability and performance of electrode materials.

Table 2 Electrochemical performance data of the CS/rGO/CuO-modified Cu-PCB electrode with varying Fe_3O_4 contents using cyclic voltammetry

Fe_3O_4 (mg L^{-1})	I_{pa} (A)	I_{pc} (A)	E_{pa} (V)	E_{pc} (V)	$\lvert I_{pa}/I_{pc}\rvert$	ΔE_p
75	3.40×10^{-4}	-3.00×10^{-4}	0.22	0.05	1.133	0.17
90	3.85×10^{-4}	-3.56×10^{-4}	0.23	0.08	1.081	0.15
105	4.34×10^{-4}	-4.12×10^{-4}	0.24	0.11	1.053	0.13
120	3.92×10^{-4}	-3.68×10^{-4}	0.26	0.10	1.065	0.16

Table 3 Determination of optimal scan rate based on the I_{pa} and I_{pc} values

Scan rate (mV s^{-1})	I_{pa} (A)	I_{pc} (A)	E_{pa} (V)	E_{pc} (V)	$\lvert I_{pa}/I_{pc}\rvert$	ΔE_p
100	5.10×10^{-4}	-4.76×10^{-4}	0.25	0.09	1.07	0.16
75	3.50×10^{-4}	-4.12×10^{-4}	0.24	0.11	1.05	0.13
50	4.34×10^{-4}	-3.34×10^{-4}	0.24	0.09	1.04	0.15
25	2.52×10^{-4}	-2.40×10^{-4}	0.23	0.06	1.05	0.17

The CS/rGO/Fe_3O_4-modified Cu-PCB electrode was tested in PBS solution (pH 7) using the CV approach. Furthermore, determination of the optimum scan rate for the produced working electrode was performed at scan rates from 25 to 100 mV s^{-1} with an increment of 25 mV s^{-1} within a potential range of −1.0 V to +1.0 V. The selected potential range was chosen to cover the redox activity of the modified electrode without causing electrochemical degradation, while the variation in the scan rate was applied to observe the effect on electron-transfer kinetics and peak current response. This approach enables the identification of the most appropriate scan rate that provides a clear and stable voltammetric signal, thereby ensuring the reliable electrochemical performance of the CS/rGO/Fe_3O_4-modified Cu-PCB electrode. The peak current responses are depicted in Fig. 8a, while the obtained parameters are summarized in Table 3.

As presented in Table 3, as the scan rate increases, the anodic (I_{pa}) and cathodic (I_{pc}) peak currents show an increasing trend, indicating an increase in the electrochemical response. Next, the $|I_{pa}/I_{pc}|$ ratio is in the range of 1.04–1.07, close to the ideal value, but the small deviation indicates that the system is not fully reversible. A shift in the peak potential is also observed, where the anodic peak potential (E_{pa}) shifts to a more positive direction and the cathodic peak potential (E_{pc}) to a more negative direction, which is characteristic of a quasi-reversible system with limited kinetics.

In addition, the peak-to-peak separation (ΔE_p) ranges from 0.13 to 0.17 V, which is significantly higher than the theoretical value of 59 mV for a reversible one-electron process. These results confirm that the electron-transfer process is quasi-reversible, with moderate electron-transfer kinetics requiring additional overpotential to drive the redox reaction.[34]

Furthermore, the I_{pa} and I_{pc} values were correlated with the square root of the scan rate, and the resulting linear fits were used to estimate the electrochemical surface area (ECSA) based on the Randles–Ševčík equation (eqn (1)) as follows:[70]

$$I_p = 2.69 \times 10^5 n^{3/2} A D^{1/2} C^{1/2} \quad (1)$$

The higher R^2 values obtained for the I_p *versus* $v^{1/2}$ plots, compared to those for I_p *versus* v, indicate that the electrochemical response is governed by a diffusion-controlled process. As indicated in Fig. 8b, the CS/rGO/Fe_3O_4-modified Cu-PCB electrode showed strong linearity, with a regression line of $y = (5.1506 \times 10^{-5})x + 9.19593 \times 10^{-6}$ ($R^2 = 0.99743$) for I_{pa} and $y = -(4.7331 \times 10^{-5})x + 2.0382 \times 10^{-6}$ ($R^2 = 0.99956$).

In this case, I_p is the peak anodic current (A), n is the number of electrons involved in the redox process, A is the electroactive surface area of the WE (cm^2), D is the diffusion coefficient (cm^2 s^{-1}) of PBS (pH 7) at room temperature, C is the analyte concentration (mol cm^{-3}), and v is the scan rate (V s^{-1}).[70] Based on all the proposed electrodes, the CS/rGO/Fe_3O_4-modified Cu-PCB electrode exhibits the largest ECSA of 0.314 cm^2. This indicates the greater availability of electroactive sites and the easier mass transport of analyte molecules to the electrode interface, thereby enhancing the current response.[71] These observations reflect the strong synergistic interactions among Fe_3O_4, rGO, and chitosan at the optimal concentrations, which collectively enhance the overall electrochemical performance for sensing applications.

Furthermore, this behavior is consistent with typical non-enzymatic electrochemical systems, where both diffusion and electron-transfer kinetics influence the overall response. Overall, the modified electrode exhibits a quasi-reversible, diffusion-controlled electrochemical process with relatively stable redox behavior, making it suitable for electrochemical sensing applications.[72] Therefore, the scan rate of 75 mV s^{-1} was further used to detect Ch concentration.

3.6.3 Electrochemical performance study for the detection of cholesterol. An evaluation of the electrochemical response for cholesterol (Ch) was conducted using the CS/rGO/Fe_3O_4-modified Cu-PCB electrode with 75 mg L^{-1} Fe_3O_4. In this study, the electrochemical performance for the detection of Ch was evaluated to quantify various concentrations of Ch solution in PBS (pH 7) *via* the CV method within a potential range of −1 to 1 V at a scan rate of 75 mV s^{-1}. The cholesterol reagent concentrations were established from 100 to 300 mg dL^{-1}, with increments of 50 mg dL^{-1}. The CV approach provided the voltammograms depicted in Fig. 9a, and the electrochemical parameter values derived from the voltammogram analysis are presented in detail in Table 4.

The electrochemical measurements, as presented in Fig. 9a and Table 4, indicate that an increase in cholesterol concentration in PBS correlates with an increase in I_{pa}. At a cholesterol concentration of 100 mg dL^{-1}, the I_{pa} value was found to be 3.80×10^{-4} A; meanwhile, the I_{pa} value increased to 6.40×10^{-4} A at 300 mg dL^{-1}. This increase indicates that an increase in cholesterol concentration also results in a higher I_{pa} current response, demonstrating the sensitivity of the electrode for Ch detection. More importantly, this result shows that the CS/rGO/Fe_3O_4-modified Cu-PCB electrode effectively oxidizes cholesterol, as evidenced by the distinct oxidation peak in the voltammogram. The oxidation process of Ch on the CS/rGO/Fe_3O_4-modified Cu-PCB electrode surface occurs *via* an electron-transfer mechanism, wherein Ch molecules lose electrons and produce oxidized products.[73] More specifically, this

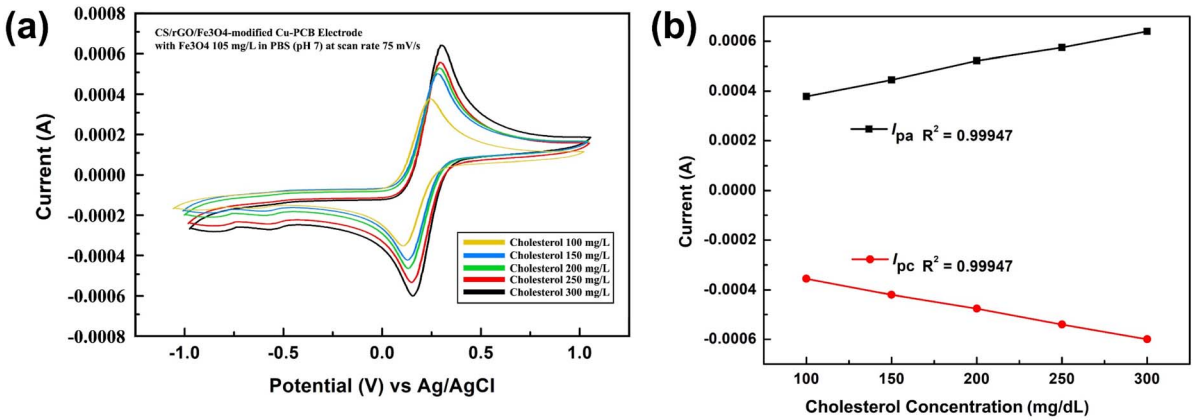

Fig. 9 (a) CV curves of the CS/rGO/Fe_3O_4-modified Cu-PCB electrode toward Ch concentration. (b) Calibration curve for Ch detection.

Table 4 Electrochemical characteristics of cholesterol detection using the CS/rGO/Fe_3O_4-modified Cu-PCB electrode

Ch (mg dL^{-1})	I_{pa} (A)	I_{pc} (A)	E_{pa}	E_{pc}	ΔE_p
100	3.80×10^{-4}	-3.55×10^{-4}	0,24	0.11	0.13
150	4.45×10^{-4}	-4.20×10^{-4}	0.26	0.12	0.14
200	5.10×10^{-4}	-4.76×10^{-4}	0.27	0.13	0.14
250	5.75×10^{-4}	-5.40×10^{-4}	0.29	0.14	0.15
300	6.40×10^{-4}	-6.00×10^{-4}	0.30	0.15	0.15

phenomenon results in the generation of protons and electrons, which are trapped by the electrode, resulting in a measurable electric current. Therefore, the modified electrode exhibits efficient electron transport.[74] The electrochemical mechanism of the proposed electrode for Ch is illustrated in Fig. S1 (see SI).

These outcomes align with several prior studies that indicated that an increase in Ch concentration correlates with an elevated I_{pa} value. Conversely, a lower Ch concentration increases the I_{pc} value and results in a larger I_{pa}/I_{pc} ratio. Therefore, the electrochemical process is irreversible, especially for the oxidation of Ch molecules on the electrode surface.[75,76] Hence, the resulting electrode can detect variations in Ch concentration. The studies on linearity, sensitivity, LOD, and LOQ will be discussed further to assess the efficacy of this electrode.

3.6.4 Linearity, sensitivity, LOD, and LOQ studies. All electrochemical measurements were carried out using independently prepared electrodes ($N = 3$) and CV detection was conducted with three consecutive sweeps for each electrode. The average value was used to measure the linearity, sensitivity, LOD, and LOQ of the developed electrode for Ch detection. The linearity was calculated using a least-squares equation, as expressed in eqn (2). In this context, y represents a dependent variable, while a, b, and x denote the slope, intercept, and Ch concentration, respectively.

$$y = a + bx. \quad (2)$$

$$\text{Sensitivity} = \frac{b}{A}. \quad (3)$$

$$\text{LoD} = \frac{3 \times \text{SD intercept}}{\text{slope}}. \quad (4)$$

$$\text{LoQ} = \frac{10 \times \text{SD intercept}}{\text{slope}} \quad (5)$$

According to the calculations derived from eqn (2), a good linear relationship was obtained with the regression equation (Fig. 9b), $I_{pa} = 2.50 \times 10^{-4} + (1.30 \times 10^{-6})x$ ($R^2 = 0.99947$) and $I_{pc} = 2.50 \times 10^{-4} + (1.30 \times 10^{-6})x$ ($R^2 = 0.99947$). Therefore, the proposed electrode exhibited a linear response in the concentration range of 100–300 mg dL^{-1}. In addition, the sensitivity of the proposed electrode was measured using eqn (3),[12] where b is the slope (A/concentration) and A is the electrode area (cm^{-2}). Based on eqn (3), the calculated sensitivity from the developed electrode for Ch is 0.160 μA μM^{-1} cm^{-2}, after normalization to

Table 5 Comparison of studies on the electrochemical detection of cholesterol

Electrode	Method	LOD (μM)	LOQ (μM)	Sensitivity (μA μM^{-1} cm^{-2})	Ref.
ChO_x/nano-MnO_2/CT/GCE	CV	2.07	NA	56	80
ZnO NRs	CV/EIS	1.78×10^3	NA	4.2	81
Ag NPs-ZnO NRs	CV/EIS	1.84×10^2	NA	135.5	81
PMO-NiO/MoS_2/SPCE	CV	6.20	20.95	0.307	32
N-GQDs/CrPic	Fluorescence	0.4	NA	NA	5
β-Cyclodextrin/Fe_3O_4	CV	2.88	NA	NA	45
CS/rGO/MnO_2	CV	0.26	0.87	3.21×10^{-5}	13
CS/rGO/Fe_3O_4	CV	0.149	0.496	0.160	This work

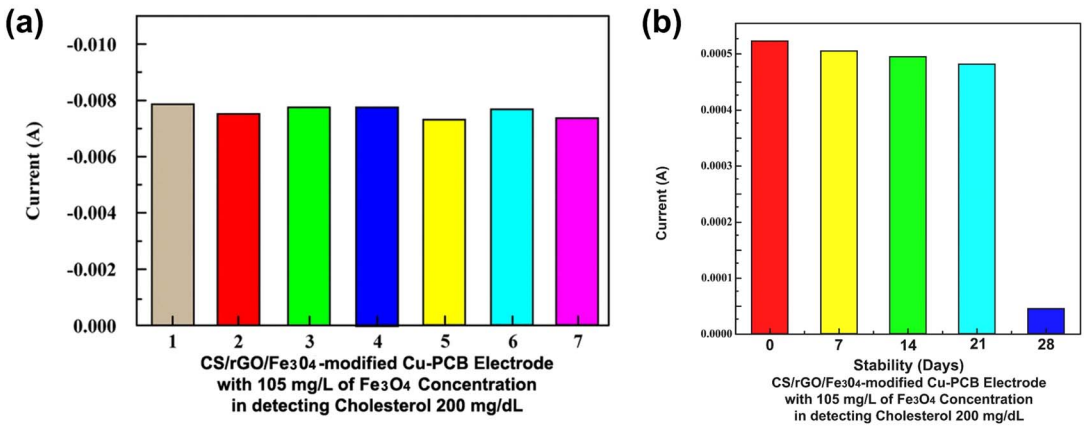

Fig. 10 (a) Reproducibility and (b) long-term stability of the CS/rGO/Fe_3O_4-modified Cu-PCB electrode for Ch detection.

the ECSA, indicating efficient utilization of the active surface for electrochemical detection.

The limit of detection (LOD) and limit of quantification (LOQ) of the proposed electrode were also determined. The LOD was calculated to evaluate the least measurable concentration of Ch, while the LOQ was determined to find the smallest quantifiable Ch concentration. Moreover, the LOD and LOQ of the Ch were computed utilising eqn (4) and (5), in which correspond to the standard deviation (SD of the intercept) of the blank signal and the slope of the calibration curve, respectively.[12] Thus, the LOD and LOQ for Ch were determined to be 0.149 μM and 0.496 μM, respectively. This relatively low LOD highlights the potential applicability of the sensor for practical cholesterol detection in biological samples. It reveals that the proposed electrode can be well applied to measure Ch concentration. Subsequently, a comparison of the electrochemical detection of Ch using different working electrodes is illustrated in Table 5.

3.6.5 Reproducibility, long-term stability, and interference studies. The reproducibility of the developed electrode was evaluated using five independently prepared electrodes, as illustrated in Fig. 10a, with detailed values provided in Table S3 (see the SI), yielding anodic peak currents (I_{pa}) in the range of 0.000516–0.000524 A with a low relative standard deviation (RSD) of 0.57%, indicating excellent fabrication consistency. The cathodic currents also showed minimal variation, while the peak potentials ($E_{pa} = 0.24$ V, $E_{pc} = 0.11$ V) and peak separation ($\Delta E_p = 0.13$ V) remained constant. These results confirm the stable electrochemical response and high reproducibility of the CS/rGO/Fe_3O_4-modified electrode for reliable sensing applications.[77]

In addition, the long-term stability of the developed electrode was evaluated over a period of 28 days by measuring the anodic peak current at regular intervals. The long-term stability results are shown in Fig. 10b and Table S4 (see the SI). The proposed electrode retained 96.7%, 94.3%, 91.6%, and 88.1% of its initial current response after 7, 14, 21, and 28 days, respectively. The gradual decrease in current response may be attributed to minor surface changes, such as partial oxidation or slight detachment of the active material over time. Despite this decrease, the electrode maintained more than 88% of its initial response after 28 days, indicating its good storage stability and structural robustness. The relatively small loss in current suggests that the composite matrix effectively preserves the electroactive sites and maintains efficient charge transfer.[78] These results demonstrate that the CS/rGO/Fe_3O_4-modified Cu-PCB electrode possesses satisfactory long-term stability, making it suitable for practical electrochemical sensing applications.

The selectivity of the developed electrode was evaluated in the presence of common interfering biomolecules, including glucose (Glu), triglycerides (Tri), uric acid (UA), and urea, at concentrations five times higher than that of cholesterol. The selectivity performance is presented in Fig. 11 along with the corresponding data in Table S5 (see the SI). The anodic peak current (I_{pa}) showed only slight deviations (<5%) compared to cholesterol alone, indicating negligible interference. The stable peak potentials and minimal change in peak separation further confirm that the electron-transfer process is not significantly

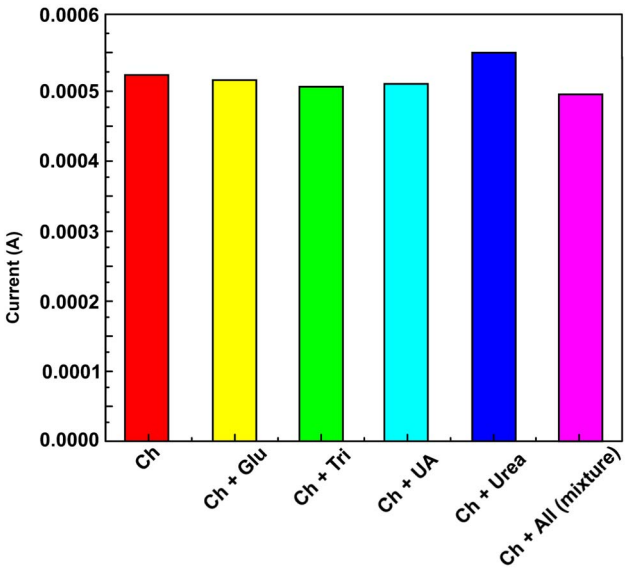

Fig. 11 Selectivity characteristics of the CS/rGO/Fe_3O_4-modified Cu-PCB electrode.

Table 6 Blood serum analysis using the proposed CV approach and comparison with medical laboratory analysis

	Ch concentration (mg dL^{-1})		
Sample	CV method (R)	Medical lab analysis (S)	Difference $(R - S)/S \times 100$
a	140	145	−3.44
b	176	182	−3.29
c	200	207	−3.38
d	248	257	−3.50

affected by coexisting species.[79] Therefore, this excellent selectivity is attributed to the synergistic interactions among chitosan, rGO, and Fe_3O_4, which enhance charge transfer and minimize nonspecific interactions, making the sensor suitable for cholesterol detection in complex biological samples.

3.6.6 Electrochemical analysis of real sample. The proposed electrode was applied for measuring the Ch concentration in human blood serums. All experiments were performed in accordance with internationally recognized ethical principles, including the Nuremberg Code and the Declaration of Helsinki. The study protocol was approved by the Ethics Committee of Universitas Sumatera Utara with Approval Number: 119/KEPK/USU/2024. Furthermore, human blood samples were obtained from Drs. H. Amri Tambunan Hospital, Deli Serdang, Indonesia, and informed consent was obtained from all participants prior to sample collection. Furthermore, the detection of Ch concentration in blood serum was carried out utilising the same procedure as that employed for Ch reagent. Additionally, the preliminary detection of Ch concentration in blood serum samples was conducted in the hospital laboratory, where the samples were collected to evaluate the precision of the analytical results utilising the CV method. The results from the analysis are tabulated in Table 6. Meanwhile, the CV voltammograms and subsequent analysis of Ch concentration in the blood serum samples are presented in Fig. 12. Regarding the CV technique, all the blood serum samples were determined utilising three consecutive sweeps for each electrode. The average value was used as the final result.

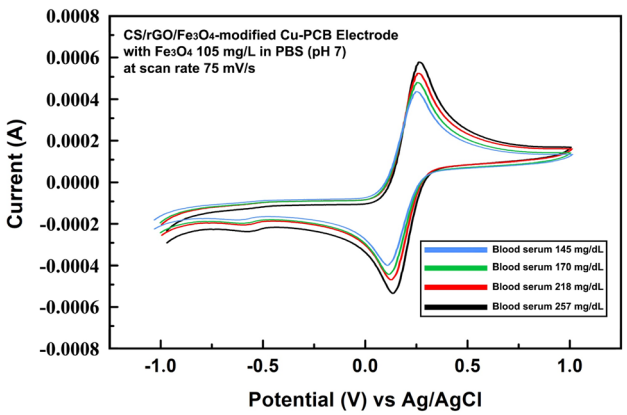

Fig. 12 CV curves of the proposed electrode toward blood serum samples.

As shown in Table 6, the findings of the Ch concentration in the blood serum samples obtained using the CS/rGO/Fe_3O_4-modified Cu-PCB electrode *via* the CV approach are relatively consistent with the laboratory analysis results. The concentration of Ch in samples a, b, c, and d was calculated to be −3.44, −3.29, −3.38, and −3.50, respectively. The electrochemical response of the serum samples showed a consistent increase in anodic peak current with an increasing cholesterol concentration. The peak current ratios ($|I_{pa}/I_{pc}| = 1.05–1.08$) and peak to peak separation values ($\Delta E_p = 0.14–0.15$ V) indicate a quasi-reversible electron-transfer process. The slight shift in peak potential with increasing concentration further confirms the expected electrochemical behavior. Although these results show small deviations compared to the laboratory analysis results, the stable peak positions and small variation in ΔE_p suggest good electrochemical stability and reproducibility in real sample analysis.

This finding aligns with prior research by Carp *et al.*[76] Conversely, the detection of Ch concentration in blood serum yielded similar results to the laboratory analysis findings. Consequently, the proposed electrode demonstrates a high degree of accuracy in quantifying the Ch concentration in blood serum using the CV-based electrochemical method and may be considered as an economical, rapid, and efficient approach for the subsequent detection of Ch concentration.

4. Conclusions

In this study, the CS/rGO/Fe_3O_4-modified Cu-PCB electrode was successfully applied as a novel strategy for non-enzymatic cholesterol measurement. The cyclic voltammetry method was used to assess the effect of Fe_3O_4 addition on detecting the cholesterol concentration in reagents and blood serum samples. The electrochemical performance studies indicated that the most suitable content of Fe_3O_4 in the CS/rGO/Fe_3O_4-modified Cu-PCB electrode is 105 mg L^{-1}. Considering the optimised setting, the proposed electrode showed a linear response within the clinically relevant range of 100–300 mg dL^{-1}, with a sensitivity of 1.30 μA (mg dL)$^{-1}$ and a low detection limit of 0.149 μM. The normalized sensitivity of 0.160 μA μM^{-1} cm^{-2} further confirms the efficient utilization of its electroactive surface. Furthermore, the proposed electrode presented good selectivity against common interfering species, excellent reproducibility (RSD = 0.57%), and satisfactory long-term stability, retaining over 88% of its initial response after 28 days. Moreover, the produced CS/rGO/Fe_3O_4-modified Cu-PCB electrode exhibited a reliable performance in human serum samples, with recovery values ranging from 96.5% to 96.7%. Overall, these results highlight the strong potential of the CS/rGO/Fe_3O_4-modified Cu-PCB electrode as a practical, stable, and reliable platform for non-enzymatic cholesterol sensing in real biological samples.

Author contributions

Irwana Nainggolan: writing–original draft, writing–review and editing, methodology, validation, conceptualization, funding

acquisition. Tulus Ikhsan Nasution: writing–review and editing, visualization, formal analysis. Sake Juli Martina: writing–review and editing, methodology. Agung Pratama: writing–review and editing, methodology, project administration. Bing Li: writing–review and editing, data curation. Maya Safrina Dalimunthe: methodology, writing–original draft. Ardiansyah Sembiring: writing–original draft, investigation, formal analysis, data curation, conceptualization, software, project administration. Reka Mustika Sari: writing–review and editing, formal analysis, data curation. Khatarina Meldawati Pasaribu: data curation, formal analysis, writing–review and editing. Hanip Fahri: methodology, data curation. Rica Asrosa: writing–review and editing. Rozyanty Rahman: writing–review and editing. Marlin Ramadhan Baidillah: data curation, writing–review and editing. Susilo Sudarman: writing–review and editing.

Conflicts of interest

The authors declare no competing financial interests or personal relationships that could have triggered the work reported in this study. Full financial support was provided to Irwana Nainggolan by the Universitas Sumatera Utara.

Data availability

The data obtained from human samples are treated as confidential and cannot be made publicly available in accordance with ethical and privacy regulations. Access to the data may be provided by the corresponding author upon reasonable request and with permission from the relevant ethics committee.

Supplementary information is available. See DOI: https://doi.org/10.1039/d5ra09147k.

Acknowledgements

The authors would like to express their sincere gratitude to the International Collaborative Research scheme of the USU TALENTA Program (Grant No. 18/UN5.4.10.S/PPM/KP-TALENTA/RB1/2024) for the financial support provided for this research. The authors also acknowledge the facilities as well as the scientific and technical assistance received from the Lampung Integrated Mineral Laboratory, National Research and Innovation Agency (BRIN), through the E-Layanan Sains platform. Furthermore, the authors extend their appreciation to Drs. H. Amri Tambunan Hospital for kindly providing the human blood serum samples and access to the analytical equipment used in this study.

References

1 J. Y. L. Chiang, J. M. Ferrell, Y. Wu and S. Boehme, Bile Acid and Cholesterol Metabolism in Atherosclerotic Cardiovascular Disease and Therapy, *Cardiol. Plus*, 2020, **5**, 159–170.

2 E. Avci, A. Dolapoglu and D. E. Akgun, *Role of Cholesterol as a Risk Factor in Cardiovascular Diseases, Cholesterol-Good, Bad and the Heart,* 2018, DOI: 10.5772/intechopen.76357.

3 World Health Federation, *Cholesterol*, 2023.

4 Kemenkes, *Kolesterol*, 2022.

5 L. Sun, S. Li, W. Ding, Y. Yao, X. Yang and C. Yao, Fluorescence detection of cholesterol using a nitrogen-doped graphene quantum dot/chromium picolinate complex-based sensor, *J. Mater. Chem. B*, 2017, **5**(45), 9006–9014, DOI: 10.1039/C7TB02037F.

6 H. Abdolmohammad-Zadeh and F. Ahmadian, A fluorescent biosensor based on graphene quantum dots/zirconium-based metal-organic framework nanocomposite as a peroxidase mimic for cholesterol monitoring in human serum, *Microchem. J.*, 2021, **164**, 106001, DOI: 10.1016/j.microc.2021.106001.

7 J. Hassanzadeh and A. Khataee, Ultrasensitive chemiluminescent biosensor for the detection of cholesterol based on synergetic peroxidase-like activity of MoS2 and graphene quantum dots, *Talanta*, 2018, **178**, 992–1000, DOI: 10.1016/j.talanta.2017.08.107.

8 M. Amirzehni, H. Eskandari, B. Vahid and J. Hassanzadeh, An efficient chemiluminescence system based on mimic CuMOF/Co_3O_4 nanoparticles composite for the measurement of glucose and cholesterol, *Sens. Actuators, B*, 2021, **348**, 130690, DOI: 10.1016/j.snb.2021.130690.

9 N. R. Nirala, P. S. Saxena and A. Srivastava, Colorimetric detection of cholesterol based on enzyme modified gold nanoparticles, *Spectrochim. Acta, Part A*, 2018, **190**, 506–512, DOI: 10.1016/j.saa.2017.09.058.

10 Y. Huang, J. Tan, L. Cui, Z. Zhou, S. Zhou, Z. Zhang, R. Zheng, Y. Xue, M. Zhang, S. Li, N. Zhu, J. Liang, G. Li, L. Zhong and Y. Zhao, Biosensors and Bioelectronics Graphene and Au NPs co-mediated enzymatic silver deposition for the ultrasensitive electrochemical detection of cholesterol, *Biosens. Bioelectron.*, 2018, **102**, 560–567, DOI: 10.1016/j.bios.2017.11.037.

11 R. Adel, S. Ebrahim, A. Shokry, M. Soliman and M. Khalil, Nanocomposite of CuInS/ZnS and Nitrogen-Doped Graphene Quantum Dots for Cholesterol Sensing, *ACS Omega*, 2021, **6**(3), 2167–2176, DOI: 10.1021/acsomega.0c05416.

12 I. Nainggolan, A. Sembiring, T. I. Nasution, R. Banurea, R. M. Sari, Andriayani, R. Rahman, B. Li, R. Asrosa and K. M. Pasaribu, A novel sensitive electrode based on a chitosan/rGO/CuO composite for the detection of urea, *RSC Adv.*, 2025, **37**, 30552–30563, DOI: 10.1039/d4ra08451a.

13 I. Nainggolan, S. J. Martina, S. Alva, B. Li, A. Sembiring, A. S. Duha, S. Saisa, R. Rahman and R. Asrosa, Sensitivity of chitosan/reduced graphene oxide/manganese dioxide modified electrodes for cholesterol detection using cyclic voltammetry, *S. Afr. J. Chem. Eng.*, 2024, **48**, 329–336, DOI: 10.1016/j.sajce.2024.03.009.

14 S. Nantaphol, O. Nantaphol and W. Siangproh, Sensitive and selective electrochemical sensor using silver nanoparticles modified glassy carbon electrode for determination of cholesterol in bovine serum, *Sens. Actuators, B*, 2015, **207**, 193–198, DOI: 10.1016/j.snb.2014.10.041.

15 M. K. Mahata, R. De and K. T. Lee, Near-infrared-triggered upconverting nanoparticles for biomedicine applications,

Biomedicines, 2021, **9**(7), 1–26, DOI: 10.3390/biomedicines9070756.

16 K. Derina, E. Korotkova and J. Barek, Non-enzymatic electrochemical approaches to cholesterol determination, *J. Pharm. Biomed. Anal.*, 2020, **191**, 113538, DOI: 10.1016/j.jpba.2020.113538.

17 H. M. Yadav, J. D. Park, H. C. Kang and J. J. Lee, Recent development in nanomaterial-based electrochemical sensors for cholesterol detection, *Chemosensors*, 2021, **9**(5), 98, DOI: 10.3390/chemosensors9050098.

18 E. N. Öven, A. Genc, N. Erk, H. E. E. Ahmed and M. Soylak, A novel NiCaAl - LDH @ ND - COOH nanocomposite - modified electrode for highly sensitive and selective electrochemical detection of larotrectinib in pharmaceutical and biological samples, *Microchem. J.*, 2025, **192**, 624, DOI: 10.1007/s00604-025-07476-4.

19 T. M. Adeniji and K. J. Stine, Nanostructure Modified Electrodes for Electrochemical Detection of Contaminants of Emerging Concern, *Coatings*, 2023, **13**(2), 381, DOI: 10.3390/coatings13020381.

20 V. Periasamy, P. N. N. Elumalai, S. Talebi, R. T. Subramaniam, R. Kasi, M. Iwamoto and G. G. Kumar, Novel same-metal three electrode system for cyclic voltammetry studies, *RSC Adv.*, 2023, **13**(9), 5744–5752, DOI: 10.1039/D3RA00457K.

21 G. Dutta, A. Regoutz and D. Moschou, Commercially Fabricated Printed Circuit Board Sensing Electrodes for Biomarker Electrochemical Detection: The Importance of Electrode Surface Characteristics in Sensor Performance, *Proceedings*, 2018, **2**(13), 741, DOI: 10.3390/proceedings2130741.

22 U. Zupančič, J. Rainbow, P. Estrela and D. Moschou, Utilising commercially fabricated printed circuit boards as an electrochemical biosensing platform, *Micromachines*, 2021, **12**(7), 793, DOI: 10.3390/mi12070793.

23 S. Mehtab, M. Zaidi and P. Joshi, Metal Nanoparticles Based Electrochemical Biosensors for Cholesterol, *J. Nanomed. Nanotechnol.*, 2020, **11**, 1–2, DOI: 10.35248/2157-7439.19.11.540.

24 D. G. A. Kariz, E. Darabi and S. M. Elahi, Electrochemical sensing of cholesterol based on MWCNTs loaded nanoparticles, *Int. Nano Lett.*, 2022, **12**, 113–123, DOI: 10.1007/s40089-021-00357-7.

25 M. Ameen Sha, P. C. Meenu, H. Haspel and Z. Konya, Metal-based non-enzymatic systems for cholesterol detection: mechanisms, features, and performance, *RSC Adv.*, 2024, **14**, 24561–24573, DOI: 10.1039/D4RA04104F.

26 R. Ahmad, K. S. Bhat, V. Nagal, U. T. Nakate, A. Akhmad, M. B. Alshammari, S. Alam and B. I. Lee, Surface-engineered vertically-aligned ZnO nanorod for sensitive non-enzymatic electrochemical monitoring of cholesterol, *Heliyon*, 2024, **10**(18), e37847, DOI: 10.1016/j.heliyon.2024.e37847.

27 N. Khaliq, M. A. Rasheed, G. Cha, M. Khan, P. Schmuki and G. Ali, Development of non-enzymatic cholesterol bio-sensor based on TiO_2 nanotubes decorated with Cu2O nanoparticles, *Sens. Actuators, B*, 2020, **302**, 127200, DOI: 10.1016/j.snb.2019.127200.

28 M. Varaminia, H. Zamani, H. Hamedania, S. Namdari and B. Rastegari, Immobilization of horseradish peroxidase on lysine-functionalized gum Arabic-coated Fe_3O_4 nanoparticles for cholesterol determination, *Prep. Biochem. Biotechnol.*, 2021, **52**, 737–747, DOI: 10.1080/10826068.2021.1992780.

29 Q. Wu, L. He, Z. W. Jiang, Y. Li, Z. M. Cao, C. Z. Huang and Y. F. Li, CuO nanoparticles derived from metal-organic gel with excellent electrocatalytic and peroxidase-mimicking activities for glucose and cholesterol detection, *Biosens. Bioelectron.*, 2019, **145**, 111704, DOI: 10.1016/j.bios.2019.111704.

30 Q. Yan, R. Wu, H. Chen, H. Wang and W. Nan, Highly sensitive cholesterol biosensor based on electron mediator thionine and cubic-shaped Cu_2O nanomaterials, *Microchem. J.*, 2023, **185**, 108201, DOI: 10.1016/j.microc.2022.108201.

31 R. Ji, L. Wang, G. Wang and X. Zhang, Synthesize Thickness Copper (I) Sulfide nanoplates on Copper Rod and It's Application as Nonenzymatic Cholesterol Sensor, *Electrochim. Acta*, 2014, **130**, 239–244, DOI: 10.1016/j.electacta.2014.02.155.

32 H. A. Ariyanta, T. A. Ivandini and Y. Yulizar, Poly(methyl orange)-modified NiO/MoS_2/SPCE for a non-enzymatic detection of cholesterol, *FlatChem*, 2021, **29**, 100285, DOI: 10.1016/j.flatc.2021.100285.

33 L. Rao, J. D. Rodney, S. Sushmitha, F. J. Mascarenhas, M. P. Nayak, B. C. Kim and B. R. Bhat, Pd/C-decorated SnO_2 for advanced non-enzymatic cholesterol biosensing: analytical application in clinical blood specimens, *Microchem. J.*, 2025, **212**, 113371, DOI: 10.1016/j.microc.2025.113371.

34 A. Hardiansyah, R. F. Maulana, N. L. W. Septiani, C. Y. Su, H. W. Fang, A. Hermawan, A. Sabarudin, Y. W. Cheng, C. Y. Kuo, T. Kida and T. Y. Liu, Chitosan/Fe_3O_4/graphene nanoplatelets composites-modified glassy carbon electrode for highly sensitive electrochemical detection of dopamine, uric acid, and ascorbic acid, *Carbohydr. Polym.*, 2026, **382**, 125245, DOI: 10.1016/j.carbpol.2026.125245.

35 A. T. Lawal, Recent developments in electrochemical sensors based on graphene for bioanalytical applications, *Sens. Bio-Sens. Res.*, 2023, **41**, 100571, DOI: 10.1016/j.sbsr.2023.100571.

36 A. Paz de la vega, F. Liendo, B. Pichún, J. Penagos, R. Segura and M. J. Aguirre, Electrochemically Reduced Graphene Oxide Covalently Bound Sensor for Paracetamol Voltammetric Determination, *Int. J. Mol. Sci.*, 2025, **26**(9), 1–17, DOI: 10.3390/ijms26094267.

37 M. Shahzad, F. Ahmad, M. Ibraheem, A. Shakoor, S. M. Ramay, M. R. Raza and S. Atiq, Tuning diffusion coefficient, ionic conductivity, and transference number in rGO/$BaCoO_3$ electrode material for optimized supercapacitor energy storage, *RSC Adv.*, 2025, **15**(8), 6308–6323, DOI: 10.1039/D4RA08894H.

38 F. Ahmad, M. Zahid, H. Jamil, M. A. Khan, S. Atiq, M. Bibi, K. Syahbaz, M. Adnan, M. Danish, F. Rasheed, H. Tahseen, M. J. Sabbir, M. Bilal and A. Samreen, Advances in graphene-based electrode materials for high-performance supercapacitors: A review, *J. Energy Storage*, 2023, **72**, 108731, DOI: 10.1016/j.est.2023.108731.

39 R. Painuli, C. Kumar and D. Kumar, Carbon nanotubes and graphene nanomaterials for biomedical applications, in *Design, Principle and Application of Self-Assembled Nanobiomaterials in Biology and Medicine*, 2022, pp. 215–226, DOI: 10.1016/B978-0-323-90984-6.00005-2.

40 S. Phetsang, A. Phengdaam, C. Lertvachirapaiboon, R. Ishikawa, K. Shinbo, K. Kato, P. Mungkornasawakul, K. Ounnunkad and A. Baba, Investigation of a gold quantum dot/plasmonic gold nanoparticle system for improvement of organic solar cells, *Nanoscale Adv.*, 2019, **1**(2), 792–798, DOI: 10.1039/C8NA00119G.

41 V. R. Feig, Tran, M. Lee, K. Liu, Z. Huang, L. Beker, D. G. Mackanic and Z. Bao, An Electrochemical Gelation Method for Patterning Conductive PEDOT:PSS Hydrogels, *Adv. Mater.*, 2019, **31**(39), 1902869.

42 D. Li, S. Wu, Q. Wang, Y. Wu, W. Peng and L. Pan, Ag @ C Core – Shell Colloidal Nanoparticles Prepared by the Hydrothermal Route and the Low Temperature Heating – Stirring Method and Their Application in Surface Enhanced Raman Scattering, *J. Phys. Chem. C*, 2012, **116**(22), 12283–12294.

43 T. Guan and N. Zhang, Recent Advances in Electrodeposition of Nickel-Based Nanocomposites Enhanced with Lubricating Nanoparticles, *Nanomanuf. Metrol.*, 2024, **7**, 25.

44 D. B. Bailmare, B. V. Malozyomov and A. D. Deshmukh, Electrodeposition of porous metal-organic frameworks for efficient charge storage, *Commun. Chem.*, 2024, **7**, 1–11.

45 S. Willyam, E. Saepudin and T. Ivandini, β-cyclodextrin/Fe_3O_4 Nanocomposite for an Electrochemical Non-Enzymatic Cholesterol Sensor, *Anal. Methods*, 2020, **12**, 3454–3461.

46 R. Doaga, T. McCormac and E. Dempsey, Functionalized magnetic nanomaterials for electrochemical biosensing of cholesterol and cholesteryl palmitate, *Microchim. Acta*, 2020, **187**, 225.

47 M. A. F. Nasution, M. I. Firmanti, H. G. Riyanto, A. R. Sanjaya, E. Saepudin and T. A. Ivandini, Electrochemical and Computational Studies of Citrate-modified β-cyclodextrin@Fe_3O_4 Nanocomposite as a Nonenzymatic Sensor for Cholesterol, *Sens. Mater.*, 2023, **35**, 4215–4234.

48 A. Sembiring, I. Nainggolan and A. Andriayani, Preparation and Characterization of Chitosan/Reduced Graphene Oxide Film as a Sensing Material, *J. Technomaterial Phys.*, 2023, **5**(2), 93–98, DOI: 10.32734/jotp.v5i2.13306.

49 I. Nainggolan, S. J. Martina, T. I. Nasution, A. Sembiring and R. N. A. Maha, The Characterization of Screen-Printed Copper Electrodes Modified with Chitosan/Reduced Graphene Oxide for Epinephrine Detection, *J. Phys.: Conf. Ser.*, 2024, **2733**, 012012, DOI: 10.1088/1742-6596/2733/1/012012.

50 N. T. A. Thu, H. V. Duc, N. H. Phong, N. D. Cuoang, N. T. V. Hoan and D. Q. Khieu, Electrochemical Determination of Paracetamol Using Fe_3O_4/Reduced Graphene-Oxide-Based Electrode, *J. Nanomater.*, 2018, **2018**, 7619419, DOI: 10.1155/2018/7619419.

51 S. Aghris, M. Azriouil, F. E. Ettadili, A. Loukili, F. Laghrib, A. Farahi, M. Bakasse, F. Lahrich and M. A. E. Mhammedi, An electrochemical sensor for flubendiamide insecticide analysis based on chitosan/reduced graphene oxide, *Sens. Diagn.*, 2023, **2**, 398–408.

52 S. Dervin, P. Ganguly and R. S. Dahiya, Disposable Electrochemical Sensor Using Graphene Oxide-Chitosan Modified Carbon-Based Electrodes for the Detection of Tyrosine, *IEEE Sens. J.*, 2021, **21**, 26226–26233.

53 S. Si, A. Kotal, T. K. Mandal, S. Giri, H. Nakamura and T. Kohara, Size-controlled synthesis of magnetite nanoparticles in the presence of polyelectrolytes, *Chem. Mater.*, 2004, **16**(18), 3489–3496.

54 C. T. Thanh, N. H. Binh, P. N. D. Duoc, V. T. Thu, P. V. Trinh, N. N. Anh, N. V. Tu, N. V. Tuyen, N. V. Quynh, V. C. Tu, B. T. V. Thao, P. D. Thang, H. Abe and N. V. Chuc, Electrochemical Sensor Based on Reduced Graphene Oxide/Double-Walled Carbon Nanotubes/Octahedral Fe_3O_4/Chitosan Composite for Glyphosate Detection, *Bull. Environ. Contam. Toxicol.*, 2021, **106**, 1017–1023.

55 A. Noorbakhsh, M. Khakpoor, M. Rafieniya, E. Sharifi and M. Mehrasa, Highly Sensitive Electrochemical Hydrogen Peroxide Sensor Based on Iron Oxide-Reduced Graphene Oxide-Chitosan Modified with DNA-Celestine Blue, *Electroanalysis*, 2017, **29**(4), 1113–1123, DOI: 10.1002/elan.201600660.

56 M. Baghayeri, H. Veisi, S. Farhadi, H. Beitollahi and B. Maleki, Ag nanoparticles decorated Fe_3O_4/chitosan nanocomposite: synthesis, characterization and application toward electrochemical sensing of hydrogen peroxide, *J. Iran. Chem. Soc.*, 2018, **15**, 1015–1022.

57 Y. H. Wang, C. M. Yu, Z. Q. Pan, Y. F. Wang, J. W. Guo and H. Y. Gu, A gold electrode modified with hemoglobin and the chitosan@Fe_3O_4 nanocomposite particles for direct electrochemistry of hydrogen peroxide, *Microchim. Acta*, 2013, **180**, 659–667.

58 S. U. Asif, A. Shakoor, B. Ashgar, A. Waheed, A. K. Alanazi, M. E. Mazhar, S. Atiq, M. Y. Haroon, Sadia, A. Qayyum, W. Abbas, Z. Bano and F. Ahmad, Design of Ni-modified ZnSe nanostructures embedded in rGO for efficient supercapacitor electrodes, *RSC Adv.*, 2025, **15**(40), 33374–33389.

59 K. Zhang, J. Helm, D. Peschel, M. Gruner, T. Groth and S. Fischer, NMR and FT Raman characterisation of regioselectively sulfated chitosan regarding the distribution of sulfate groups and the degree of substitution, *Polymer*, 2010, **51**(21), 4698–4705.

60 G. P. Mikhailov, S. V. Tuchkov, V. V. Lazarev and E. I. Kulish, Complexation of chitosan with acetic acid according to Fourier transform Raman spectroscopy data, *Russ. J. Phys. Chem. A*, 2014, **88**, 936–941.

61 Y. Kang, H. J. Kim, S. H. Lee and H. Noh, Paper-Based Substrate for a Surface-Enhanced Raman Spectroscopy Biosensing Platform—A Silver/Chitosan Nanocomposite Approach, *Biosensors*, 2022, **12**(5), 266.
62 K. Zhang, D. Peschel, J. Helm, T. Groth and S. Fischer, FT Raman investigation of novel chitosan sulfates exhibiting osteogenic capacity, *Carbohydr. Polym.*, 2011, **83**, 60–65.
63 M. Yadav, K. Y. Rhee, S. J. Park and D. Hui, Mechanical properties of Fe_3O_4/GO/chitosan composites, *Composites, Part B*, 2014, **66**, 89–96.
64 S. Zhao, M. Li, J. Ding, S. Yang, Y. Zang, Y. Zhao, X. Gao and N. Ren, Fabrication of rGO/Fe_3O_4 magnetic composite for the adsorption of anthraquinone-2-sulfonate in water phase, *Water*, 2021, **13**(17), 2315.
65 D. A. Barus, S. Humaidi, R. T. Ginting and J. Sitepu, Enhanced adsorption performance of chitosan/cellulose nanofiber isolated from durian peel waste/graphene oxide nanocomposite hydrogels, *Environ. Nanotechnol., Monit. Manage.*, 2022, **17**, 100650.
66 H. A. Ahmed, Y. A. El-Maradny, M. A. Shalaby, H. El-Menshawy and A. E. Abd EL-Wahab, Isolation and characterization of Chitosan from shrimp shell waste and the sustainable preparation of salicylic acid-loaded Chitosan nanoparticles for antibiofilm applications, *Sci. Rep.*, 2025, **15**, 1–17.
67 R. Ren, Y. Zhong, X. Ren and Y. Fan, Chitosan-based oxygen-doped activated carbon/graphene composite for flexible supercapacitors, *RSC Adv.*, 2022, **12**, 25807–25814.
68 K. Singh, N. Paliwal and K. Kasamias, Surface roughness characterization using representative elementary area (REA) analysis, *Sci. Rep.*, 2024, **14**(1785), 1–20, DOI: 10.1038/s41598-024-52329-4.
69 M. V. Scopelliti, A. Uria, A. L. Larrañaga, S. Egri, F. Jiang and L. Borgese, Performance comparison of titanium–iron flow batteries using sulfuric acid and ethylenediaminetetraacetate as complexing agents, *J. Energy Storage*, 2026, **154**(C), 121230.
70 A. K. Dhukate, S. B. Mullani, N. B. Mullani, T. D. Dongale and S. D. Delekar, Carbon nanotube integrated MOF-derived $ZnCo_2O_4$: a nanohybrid electrochemical platform for riboflavin sensing, *RSC Adv.*, 2026, **16**(18), 16601–16612.
71 N. Mohammadi, M. Bahmaei and A. M. Sharif, Highly sensitive CuZnO-Fe_3O_4/rGO modified glassy carbon electrode for the electrochemical determination of acetaminophen, tyrosine and codeine in human blood plasma and urine, *J. Electroanal. Chem.*, 2021, **902**, 115768.
72 Z. Masood, H. Muhammad and I. A. Tahiri, Comparison of Different Electrochemical Methodologies for Electrode Reactions: A Case Study of Paracetamol, *Electrochem*, 2024, **5**(1), 57–69.
73 L. Xu, Y. Hou, M. Zhang, X. Yang, G. Jenkins, W. Huang, C. Yao and Q. Wu, A novel electrochemical biosensor for detection of cholesterol, *Russ. J. Electrochem.*, 2016, **52**, 239–244.
74 M. Eghbali, F. Kheiri, M. Sirousazar, E. Jannatdoust and A. Afghan, An ultrasensitive non-enzymatic electrochemical cholesterol sensor based on copper foam/CuO/Pt/p-phenylenediamine molecularly imprinted polymer, *J. Appl. Electrochem.*, 2023, **53**, 2001–2012.
75 L. Zhang, J. Zhu, W. Hong and G. Li, Highly sensitive electrochemical detection of cholesterol based on Au–Pt NPs/PAMAM–ZIF-67 nanomaterials, *Anal. Sci.*, 2024, **40**, 37–45.
76 O. E. Carp, M. Pinteala and A. Arvinte, Innovative Non-Enzymatic Electrochemical Quantification of Cholesterol, *Sensors*, 2022, **22**(3), 828.
77 S. Chelly, M. Chelly, S. B. H. Fraj, E. Fazio, C. Corsaro, G. M. Abdullah, S. Conoci, G. Neri and D. Morganti, Screen-Printed Carbon Electrode Modified with ZrO_2/Ag/GO for Simultaneous Detection of Catechol and Hydroquinone, *Molecules*, 2026, **31**(5), 1–21.
78 A. S. Alqahtani, S. Elshafie, A. Mubarakali, A. AlJarullah, P. Parthasarathy, M. Venkatesh and S. A. Rag, Electrochemical sensor based on α-Fe_2O_3/rGO core-enhanced carbon interfaces for ultra-sensitive metronidazole detection, *Sci. Rep.*, 2025, **15**, 1–15.
79 P. V. Narayana, M. R. T, P. Gopal, K. Reddaiah and P. Raghu, Development of Electrochemical sensor based on Poly (xylenol orange) film towards the determination of L-Dopa and its simultaneous resolution in the presence of Uric acid : A cyclic Voltammetric study, *Res. J. Chem. Sci.*, 2014, **4**, 37–43.
80 C. Charan and V. K. Shahi, Nanostructured manganese oxide – chitosan-based cholesterol sensor, *J. Appl. Electrochem.*, 2014, **44**, 953–962.
81 T. T. N. Anh, H. Lan, L. T. Tam, V. H. Pham and P. D. Tam, Highly Sensitive Nonenzymatic Cholesterol Sensor Based on Zinc Oxide Nanorods, *J. Electron. Mater.*, 2018, **47**, 6701–6708.